AN ENERGY BASED MODEL FOR THE COMPRESSIVE BEHAVIOR OF GOOSE DOWN

A Dissertation
Presented to
The Academic Faculty

By

Timothy Philip Wilde

In Partial Fulfillment
Of the Requirements for the Degree
Masters of Mechanical Engineering

Georgia Institute of Technology
November, 2004

AN ENERGY METHOD APPROACH TO THE COMPRESSIVE BEHAVIOR OF GOOSE DOWN

Approved by:

David L. McDowell
School of Mechanical Engineering
Georgia Institute of Technology

Karl I. Jacob,
School of Polymer, Textile & Fiber Engineering
Georgia Institute of Technology

Richard W. Neu
School of Mechanical Engineering
Georgia Institute of Technology

Date Approved: November 2004

ACKNOWLEDGEMENT

I would like to thank Dr. Karl Jacob of for all of his help and guidance during this project. Likewise, Dr. David McDowell deserves tremendous thanks for accepting me as his graduate student and providing tremendous support through the development of this thesis. I would also like to thank Dr. Richard Neu for agreeing to be on this committee.

TABLE OF CONTENTS

LIST OF TABLES

LIST OF FIGURES

NOMENCLATURE

A_{1i}	Coordinates of fiber end in undeformed state
A_{2i}	Coordinates of fiber end in deformed state
A_j	Cross-sectional area of the fiber assembly
B	Constant associated with distribution for energy per contact
B_{1i}	Coordinates of fiber end projected into transverse plane in unstrained state
B_{2i}	Coordinates of fiber end projected into transverse plane in strained state
B_f	Fiber flexural rigidity
b	Left Cauchy-Green deformation tensor
b	Softening factor
b_R	Softening parameter for reloading
b_U	Softening parameter for unloading
b_f	Fiber bending element length
b_G	Constant associated with Gaussian distribution
b_j	Height of section considered in Carnaby *et al.* model
C	Right Cauchy-Green deformation tensor
C	Constant used in function related to evolution of contact energy distribution
C_1, C_2	Arbitrary Material Constants
C_f	Frictional force along fiber axis due to contact
C_j	Contact force in *j* direction
C_{jn}	Contact force normal to fiber axis
C_{jp}	Contact force parallel to fiber axis

C_{sj}	Contact slipping force
C_U	Constant used in determining b_U
c	Scaling factor used in contact energy distribution
D	Maximum value of the strain energy density
D_f	Fiber diameter
E_{bi}	Bending energy in the i^{th} fiber
E_{ct}	Energy per contact
$E_{ct(max)}$	Maximum energy per contact
E_{ct}^{norm}	Normalized and scaled contact energy
$E_{ct\max}^{norm}$	Maximum normalized and scaled contact energy
E_f	The Young's modulus of a fiber/secondary
E_{Si}	Slipping energy in the i^{th} fiber
E_{Ti}	Straightening energy in the i^{th} fiber
$E_{T_{jj}}$	jj component of the tangent compliance matrix
E_{tot}	Total energy stored in the fiber assembly
F	Deformation gradient
F(m;M)	Stress Softening Function
F_c	Contact force in the van Wyk model
FODF	Orientation distribution function
$g(E_{ct})$	Distribution for the energy per contact
I_3	Third strain invariant
$I_i(\mathbf{b})$	i^{th} invariant of the based on the Left Cauchy-Green deformation tensor
I_f	Fiber Moment of Inertia

I_j	Orientation related parameter used
I_o	Orientation factor
$J(\boldsymbol{\varepsilon},\boldsymbol{o})$	Function related to the FODF for a given strain and fiber defined by **o**
K	Material constant for van Wyk model
K_d	Dynamic bulk modulus of fiber mass
K_j	Orientation related factor
k_b	Boltzmann's constant
L^{-1}	Inverse Langevin function
L_f	Total length of fiber per unit volume
l	Bond length in a molecular chain
l_f	Secondary length
l_{1i}	Length of the i^{th} fiber in unstrained state
l_{2i}	Length of the i^{th} fiber in strained state
M	Maximum strain intensity
M^*	Maximum strain intensity in the *deformed* configuration
m	Strain intensity
m^*	Strain intensity in the *deformed* configuration
m_f	Mass of fibers in the van Wyk model
m_{jj}	Orientation related quantity from Carnaby *et al.* (1989)
N	Constant used in proposed model
N_{TT}	Number of tertiary-to-tertiary engagements
N_B	Number of fibers undergoing bending
N_{ch}	Number of molecular chains per unit volume

N_S	Number of contacts slipping
N_T	Number of fibers that are straightening
N_{TT}	Number of tertiary-to-tertiary contacts per unit volume
n	Number of bonds in a single molecular chain
n_{bj}	Number of contacts in section of height b_j
$\bar{n}_v$	Average number of contacts per unit volume
ODF	Orientation distribution function
$\mathbf{o}_i$	Fiber components in i^{th} direction
P	Nominal stress
$\bar{P}$	Applied external pressure
P_i	The i^{th} principal nominal stress
$-\Delta\bar{P}$	Change externally applied pressure
$\Delta\mathbf{P}_0$	Incremental change in nominal stress
PSOE	Primary structure orientation ellipsoid
p(x,y,z)	Probability of a chain end being located at x,y,z
R	Rotation tensor
R	Radius of curvature of deformed secondary structure
RVE	Representative volume element
r_o	End-to-end distance of molecular chain in *initial* configuration
r	End-to-end distance of molecular chain in *current* configuration
S	Total entropy of a molecular chain network
S	Entropy of a single molecular chain
SN	Number of slipping contacts

$\mathbf{S}_T(\mathbf{P}_0, \boldsymbol{\varepsilon}_0)$	Tangent compliance matrix relating stress and strain
$\mathbf{T}$	Cauchy Stress Tensor
T	Temperature
T_i	The i^{th} principal Cauchy stress in *current* configuration
T_i^o	The i^{th} principal Cauchy stress in the *original* configuration
$\mathbf{T}^o$	Cauchy stress in the initial compression of the *virgin* material
$\mathbf{T}^{o\ max}$	Maximum Cauchy stress in the initial compression of the *virgin* material
$\hat{\mathbf{T}}_o$	Scaled stress
$\hat{\mathbf{T}}^{o\max}$	Scaled maximum stress
$\mathbf{U}$	Right Stretch tensor
V_0	Volume of fiber mass in the unstrained state
V	Current volume of the fiber mass
WF_o	Withdrawal force in unstressed state
x_o, y_o, z_o	Coordinate for free end of molecular chain in *initial* configuration
x, y, z	Coordinate for free end of molecular chain in *current* configuration
α_1, α_2	Exponent in equation for N_{TT}
α_p	Constant in the Ogden model
α_U	Exponent dictating evolution of b_U
β	Constant related to initial density of goose down material
$\beta_{L^{-1}}$	Result of inverse Langevin function
χ	Angle between two fibers
δ	Fiber deflection

ε_{max}	Maximum strain
$\Delta\boldsymbol{\varepsilon}$	Incremental change in strain
$\delta\varepsilon_{ii}$	Incremental change of *ii* strain component
ϕ	Azimuthal angle
ϕ'	Azimuthal angle of contact fiber
ϕ^*	Azimuthal angle in deformed configuration
γ	Exponent in PSOE equations, influence change in orientation
η_f	Fiber shape parameter relating to fiber cross-section shape
η_i	Primary structure orientation parameter associated with i^{th} principal stretch direction
η_{io}	Initial i^{th} ratio of the primary structure orientation ellipsoid axes
max η_i	Maximum of three ratios defined by η_i
λ_i	Principal stretch in the i^{th} principal direction referenced to the *undeformed* configuration
λ_i'	Principal stretch in the *original* configuration corresponding to a principal stretch in the *new* configuration.
λ_i^{max}	Maximum principal stretch in the i^{th} principal direction
λ_i^*	Principal stretch in the i^{th} principal direction referenced to the *deformed* configuration
λ_i^{*max}	Maximum principal stretch in the i^{th} principal direction referenced to the *deformed* configuration.
λ_i^R	Reversible principal stretch in the i^{th} principal direction
λ_i^{IR}	Irreversible principal stretch in the i^{th} principal direction
μ	Shear modulus referred to the reference configuration
μ_{fr}	Static coefficient of friction between fibers

θ	Polar angle
θ_{1i}	Polar angle of the i^{th} fiber in unstrained state
θ_{2i}	Polar angle of the i^{th} fiber in strained state
θ'	Polar angle of contacting fiber
θ^*	Polar angle of fiber after deformation
ρ	Bulk density of a fiber assembly
ρ_f	Individual fiber density
ρ_T	Tertiary density
σ_i	The i^{th} principal stress
σ_{max}	The maximum stress
$\mathbf{\Omega}_P$	Primary structure fabric tensor
$\Omega(\theta,\phi)$	Fiber orientation distribution function
ϖ_i	Principal values of the primary structure fabric tensor
$\omega°$	Solid angle
ω_{i0}	Initial magnitude of the i^{th} principal axis of the PSOE
ω_i	Magnitude of the i^{th} principal axis of the PSOE
ξ	Damage variable
$\Psi(\mathbf{F})$	Strain-energy function based on deformation gradient
$\Delta\Psi$	Incremental change in stored elastic strain-energy

SUMMARY

There are many products used in everyday life that are made from materials consisting of a loose network of natural or synthetic fibers. Some common examples of these materials are carpets, felts, wool and *goose down*. In many cases, the resilience of these materials under cyclic loading influences the product's lifespan and value.

In most end-uses, these products are exposed to repeated compressive loadings that eventually result in a loss of performance. When tested in a piston-cylinder device, these materials usually exhibit some irreversible deformation and hysteresis; two behaviors that can be difficult to adequately capture in a model.

Goose down is one of the most desirable materials for these applications because of its superior insulating capability and phenomenal lofting performance. These characteristics make goose down the preferred fill material for luxury comforters and pillows and, in turn, make it extremely valuable in the consumer market.

Despite the value of goose down in the consumer market, very little work has been done to study its mechanical properties and develop an associated model. This thesis focuses on developing a model for the compressive behavior of goose down. First, the morphology of goose down is explored in order to gain insight into the key mechanisms that influence its compressive response. Assumptions regarding the influence of the down structure on performance are then incorporated into a strain-energy function which can be implemented into a modified hyperelastic constitutive framework to determine the principal stresses of the material while capturing the hysteresis and irreversible deformation observed in piston-cylinder tests.

CHAPTER I

INTRODUCTION

There are many products used in everyday life that are made from materials consisting of a loose network of natural or synthetic fibers. Some common examples of these materials are carpets, felts, wool and goose down. In many cases, the resilience of these materials under cyclic loading influences the product's lifespan and value.

In most applications these products are exposed to repeated compressive loadings that eventually result in degradation and loss of performance. When tested in a piston-cylinder device, these materials usually exhibit some irreversible deformation and hysteresis (Figure 1.1.1); two behaviors that can be difficult to adequately capture in a model.

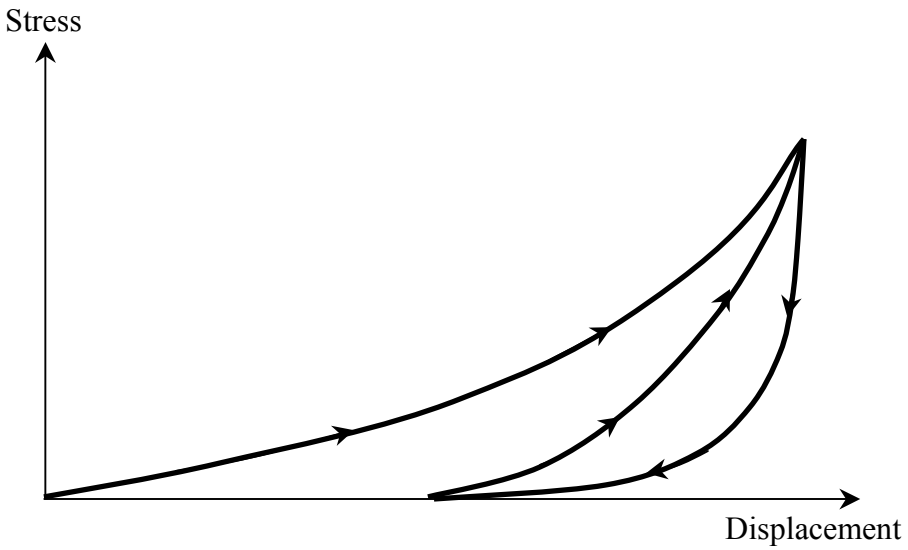

Figure 1.1.1 A typical response of a fill material subject to compression in a piston-cylinder device. Loading, unloading, and reloading curves shown

Despite the large demand and economic value of these products, an adequate model for these materials has not been developed. Most attempts to model their behavior have focused on determining the stored elastic strain-energy from the micromechanics that dictate fiber-to-fiber interactions. These fiber interactions can then be related to the overall fiber network stiffness and the material response can be evaluated. While these models are moderately successful, they become complicated and difficult to implement.

Goose down is one of the most desirable materials for these applications because of its superior insulating capability and phenomenal lofting performance. These characteristics make goose down the preferred fill material for luxury comforters and pillows and, in turn, make it extremely valuable in the consumer market. Despite the value of goose down in the consumer market, very little work has been done to study its mechanical properties, understand the underlying mechanisms, and develop an associated model. This thesis focuses on developing a preliminary model for the compressive behavior of goose down. First, the morphology of goose down is explored in order to gain insight into the key mechanisms that influence its compressive response. Assumptions regarding the influence of goose down structure on performance are then incorporated into a strain-energy function which can be implemented into a modified hyperelastic constitutive framework to determine the principal stresses of the material while capturing the hysteresis and irreversible deformation observed in piston-cylinder tests. The proposed model for goose down is them evaluated for uniaxial compression and shown to capture the essence of the observed behavior.

CHAPTER II

GOOSE DOWN MORPHOLOGY

2.1 General Goose Down Information

Despite significant advances in polymer and textile materials design, naturally occurring fiber networks remain unmatched in terms of resilience and insulating abilities. Quality goose and duck down continue to be the premium fill material for many bedding and clothing products. Goose and duck down come from the breast area of the waterfowl and provide insulation from cold weather and water. While dramatically improved, synthetic materials cannot match the lofting performance of quality duck and goose down on a per mass basis. Lofting, also known as fill power, is concerned with the ability of a given mass of material to occupy a volume.

Fill power is the most common parameter used to distinguish between different grades of goose down used in consumer products. A material with a higher fill power is able to occupy a greater volume with a smaller mass and in turn offers greater insulating capabilities. Because fill power has a strong influence on product value, strict guidelines and testing procedures exist to ensure that product labeling and performance concur.

The International Down and Feather Laboratory (IDFL) conducts much of the testing and ranking of raw down materials imported from around the world for sale in the United States. A piston-cylinder system is used to determine the fill power. The exact specifications and procedures for this test are available at the IDFL website (IDFL 2004). There are different standards for testing around the world; however, the interpretation and testing principles remain unchanged.

The *content* of a down sample is extremely important as it also influences the fill power. In this context, content typically refers to the percentage of pure down clusters (Figures 2.2.2&3) compared to the quantity of other materials found in a sample. Dirt, broken and whole feathers, residue, and down fiber are commonly present along with down clusters and cause adverse effects on performance. It is extremely important to note that there are significant structural differences between feathers and down clusters that will be shown in detail later. Based on data recorded by the IDFL, shown in Figure 2.1.1, there is a correlation between down content and average fill power, where multiple samples have been tested for each content level over years of testing.

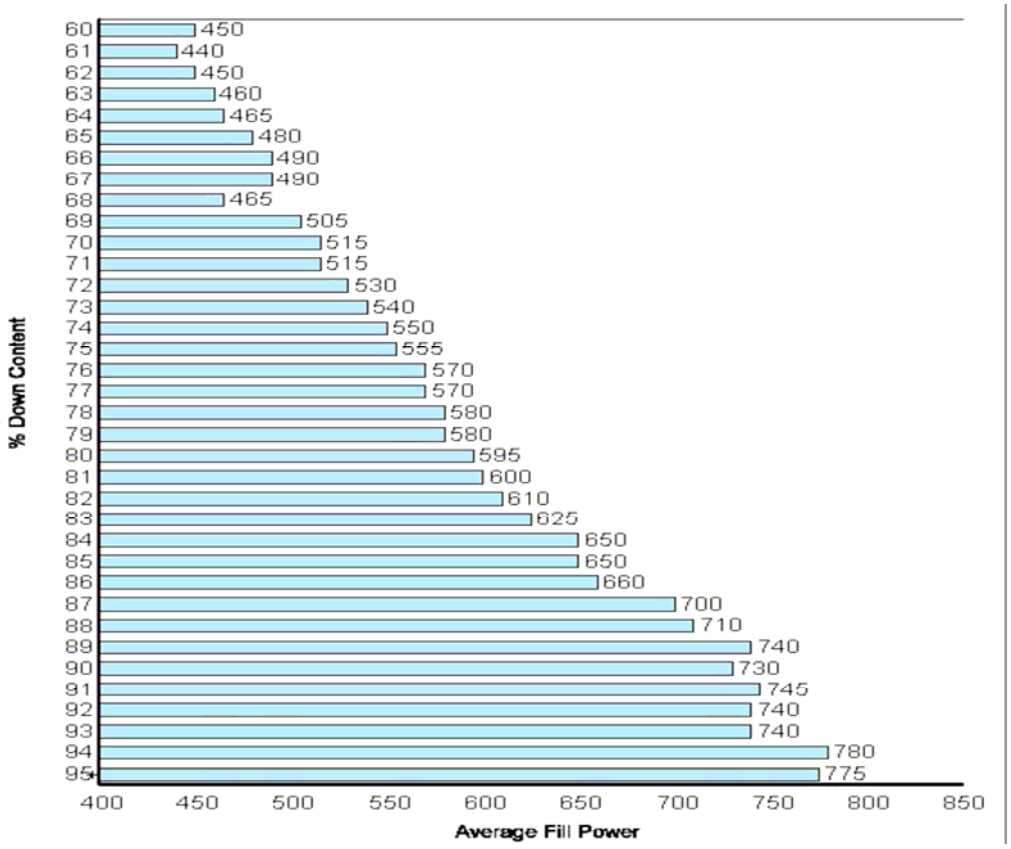

Figure 2.1.1 Relation between fill power and % down content from tests completed by the IDFL.

Other factors, such as color, odor, and cleanliness are important for determining the value of down, but these elements do not correlate directly with the mechanical properties whereas fill power and content are critical.

With this general understanding of where goose down originates and how its value in the consumer world is measured, it is now necessary to explore the morphology of down. By studying the structure one can gain valuable insight into the mechanisms that allow this organic material to outperform man-made products. First, goose down will be explored at the macro scale and then on the micro scale. Efforts have been made to examine the behavior in both dynamic and static settings to further identify and understand the relevant mechanisms. Image processing to determine lengths and deformations was performed using the freeware UTHSCSA Image Tool (UTHSCSA 2002).

2.2 Macroscopic Goose Down Observation

The immediate inspection of down reveals that the material consists of clusters (Figure 2.2.1) that typically range in size from 5.0 mm to 70.0 mm in "diameter". These clusters are somewhat spherical in shape when they are suspended freely in the air. They have a central node, or root, with many strands extending outward in all directions. Departing from these strands are very fine structures (Figure 2.2.2) resembling whiskers or "fuzz". For consistency, these fine structures will be referred to as *secondary* structures, while the main branches will be called *primary* structures.

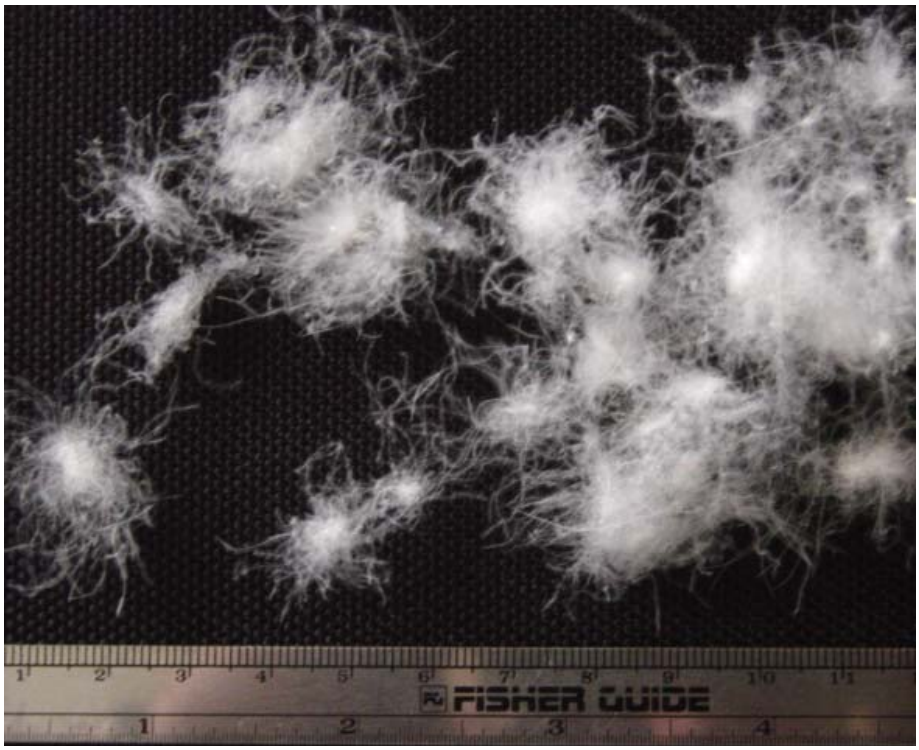

Figure 2.2.1 Goose down clusters of varying size. Scale in cm.

Figure 2.2.2 A single goose down cluster, showing primary branches with feathery secondary structures. Scale in cm.

As mentioned above, feathers can also be present in varying sizes as show in Figure 2.2.3. Feathers are two-dimensional structures and look more like the flight feathers. In some cases the main stem of a feather can be stiff stem which can penetrate encapsulating fabrics. Down samples with higher feather quantities usually exhibit a lower fill power performance, suggesting that they are not desired in for optimal performance.

Figure 2.2.3 Feathers of various sizes from a 500 fill power sample of goose down. Scale in cm.

The differences between down and polyester fill are obvious even at the macroscopic level. Figure 2.2.4 shows a typical fill material used in couch cushions. The polymer fill material is made of smooth filaments that are not bonded together in any way. This fiber arrangement differs from the multi-scale structure of goose down. Furthermore, the polymer fibers are typically longer than the down primary structures and makes them more prone to becoming permanently entangled. In order to maintain

loft, synthetic fibers are crimped, meaning that they are not straight and will follow a "zigzag" pattern. The tensile strength of man-made materials is typically higher; however, very little tensile forces are generated within the material during compression and recovery. Therefore, little elastic strain energy is stored in the fibers due stretching compared to the energy induced to due to bending.

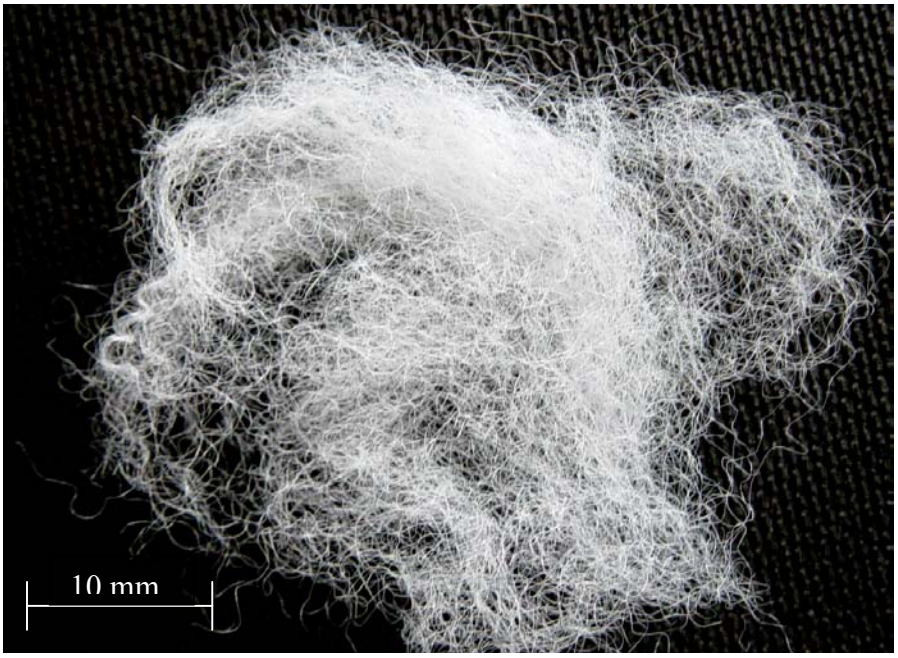

Figure 2.2.4 Polyester fill material from a couch cushion.

The macroscopic perspective has illustrated several differences between goose down and synthetic materials. The hierarchically branched structure of goose down contributes to its superior resilience. Further exploration at a finer microscopic scale can provide further insight into other structural properties that may be important in developing a more realistic model for goose down.

2.3 Static Microscopic Exploration

Low magnification optical microscopy was used for fine scale observations. All micrographs were obtained using an Olympus BX 40 optical microscope connected to a Sony CCD-IRIS digital camera. Images were captured to a PC using the Epix Inc. XCAP Lite software. The images were taken using the dark-field configuration in order to optimize the image contrast.

Studying these clusters with a microscope shows that they consist of a main root with a sturdy stem protruding from it. The primary structures mentioned above branch from this stem outward in all directions so that they take the general shape of a sphere. (Figures 2.3.1 and 2.3.2) The primary length was measured for 40 randomly selected clusters and was found to vary between 5.0mm and 32.8mm with an average length of 20.0mm. The 40 samples were selected from different clusters since the primary, secondary, and tertiary structures were found to be consistent for a given cluster.

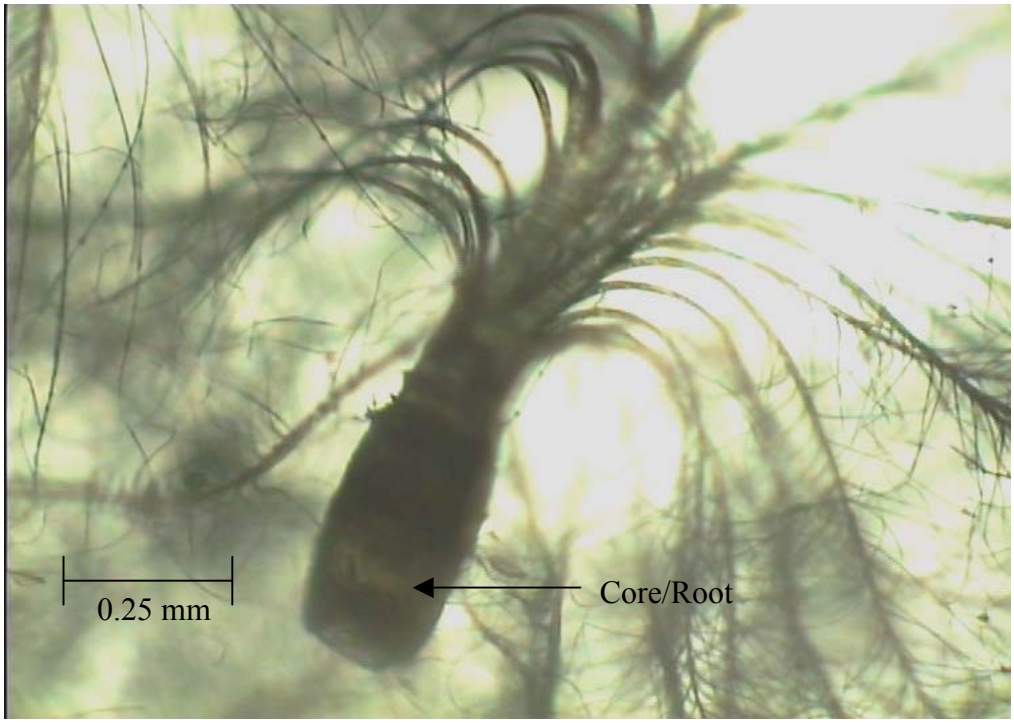

Figure 2.3.1 Micrograph showing the main root of a goose down cluster.

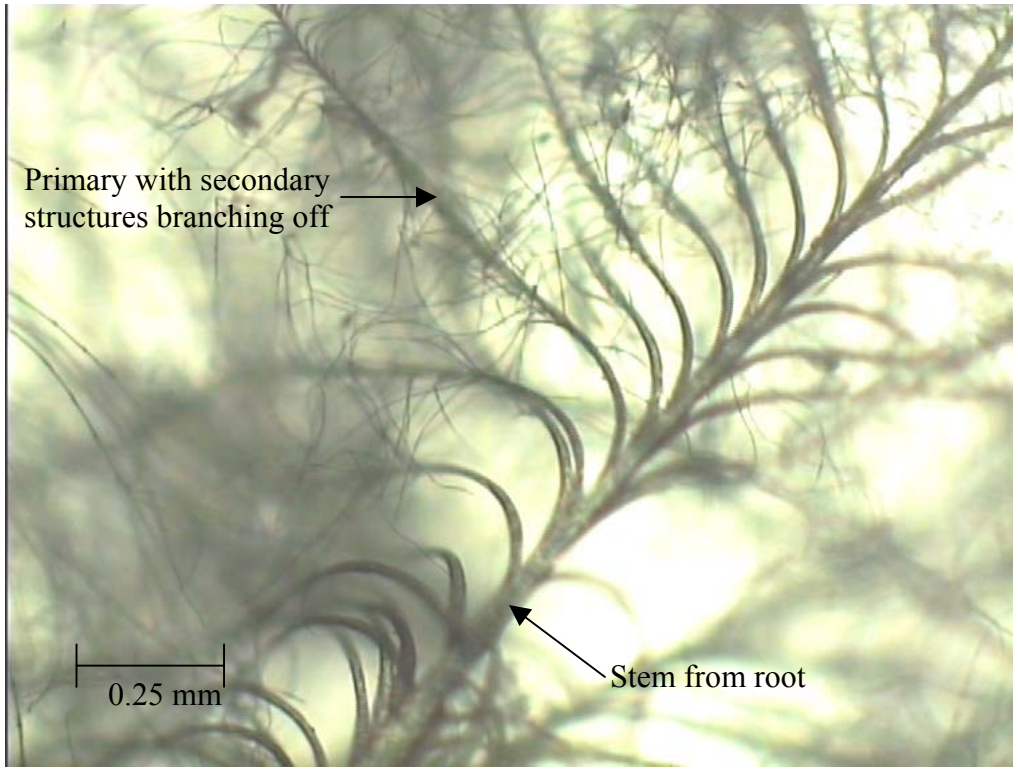

Figure 2.3.2 Micrograph showing the stem which protrudes from the main root (Figure 2.3.1)of a goose down cluster. Primaries depart from the stem with secondaries branching from primaries.

Further examination of the primary structures reveals secondary structures that branch out radially with a nearly periodic spacing. On average, the spacing between secondary structures was 0.06 mm. The secondary lengths ranged between 0.35 mm and 1.386 mm with an average length of 0.65 mm. These secondary fibers impart to down its remarkable spring back from repeated compression. Secondaries exhibit a tremendous ability to rebound completely from high degrees of bending. Figure 2.3.3 shows a close-up of the primary structure with the secondary structures branching off radially. The solid dark "spots" present on the secondary arms are tertiary structures.

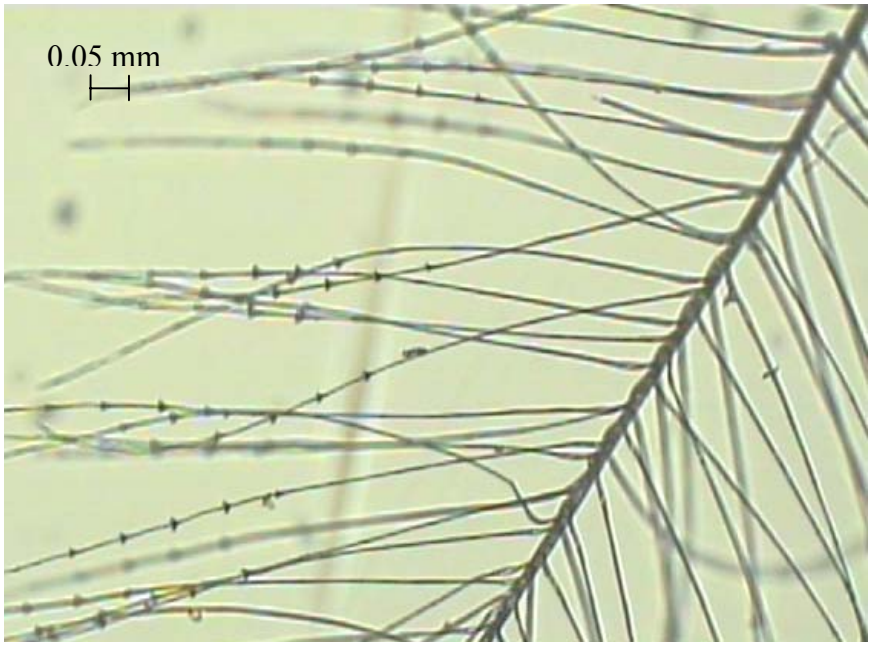

Figure 2.3.3 Primary structure with secondary structure exhibiting some tertiary structures.

These tiny bud-like structures prove to be extremely important during the compression and recovery of goose down. The tertiary structures varying in size and appear on most secondary structures in two different forms. Some tertiary structures look

like a split in the secondary branch while others are solid (Figures 2.3.4). Both versions of tertiary structures play a similar role in the compression of the fiber mass. The secondary and tertiary structures were also examined with a scanning electron microscope (SEM) as shown in Figure 2.3.5.

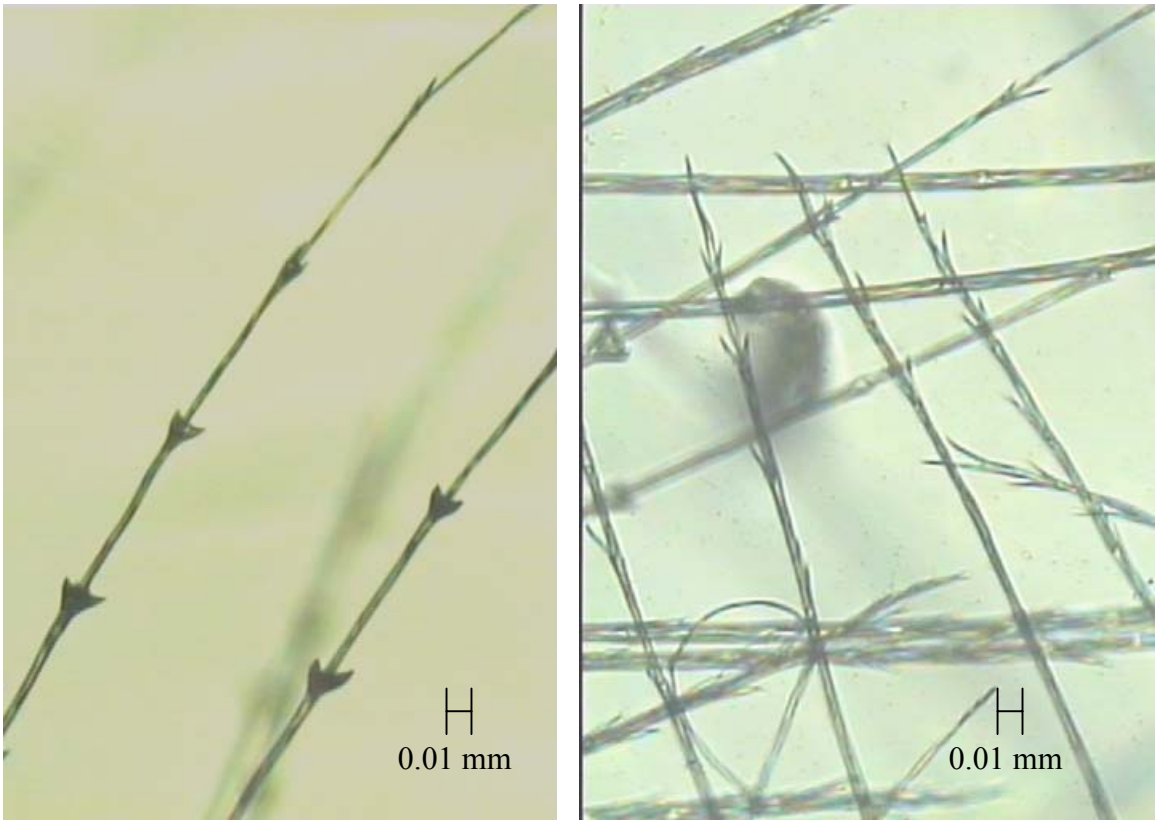

Figure 2.3.4 (a) Solid tertiary structures. (b) Split tertiary structures.

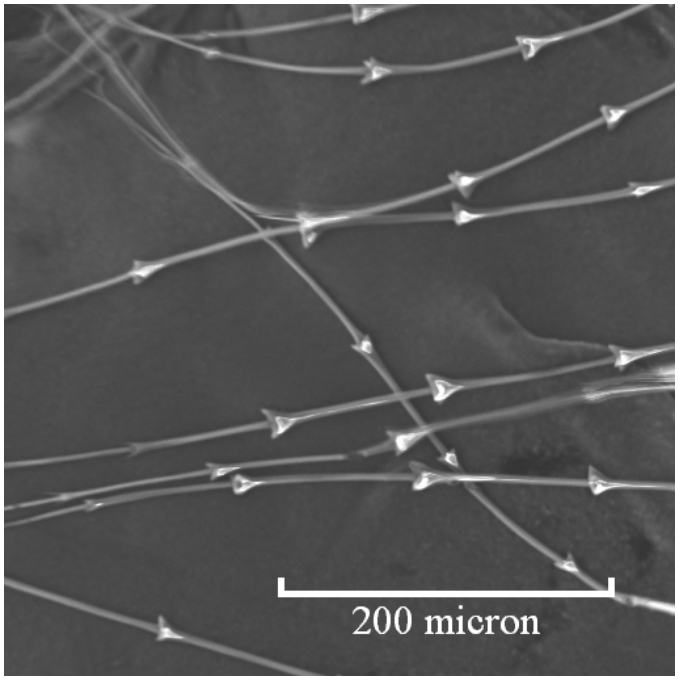

Figure 2.3.5 SEM Micrograph of secondary and tertiary structures.

As mentioned above, the secondary structures exhibit a tremendous ability to resist permanent deformation and can store a large amount of elastic energy in bending. Figures 2.3.5(A-C) show a secondary before deformation, during deformation, and finally post deformation in the recovered configuration. The fiber was displaced by sliding a small rod parallel to the primary structure. It is clear that the secondary was able to recover to its original configuration despite the high degree of deformation. The secondary structures were even observed to fully recovery after being bent into a complete circle.

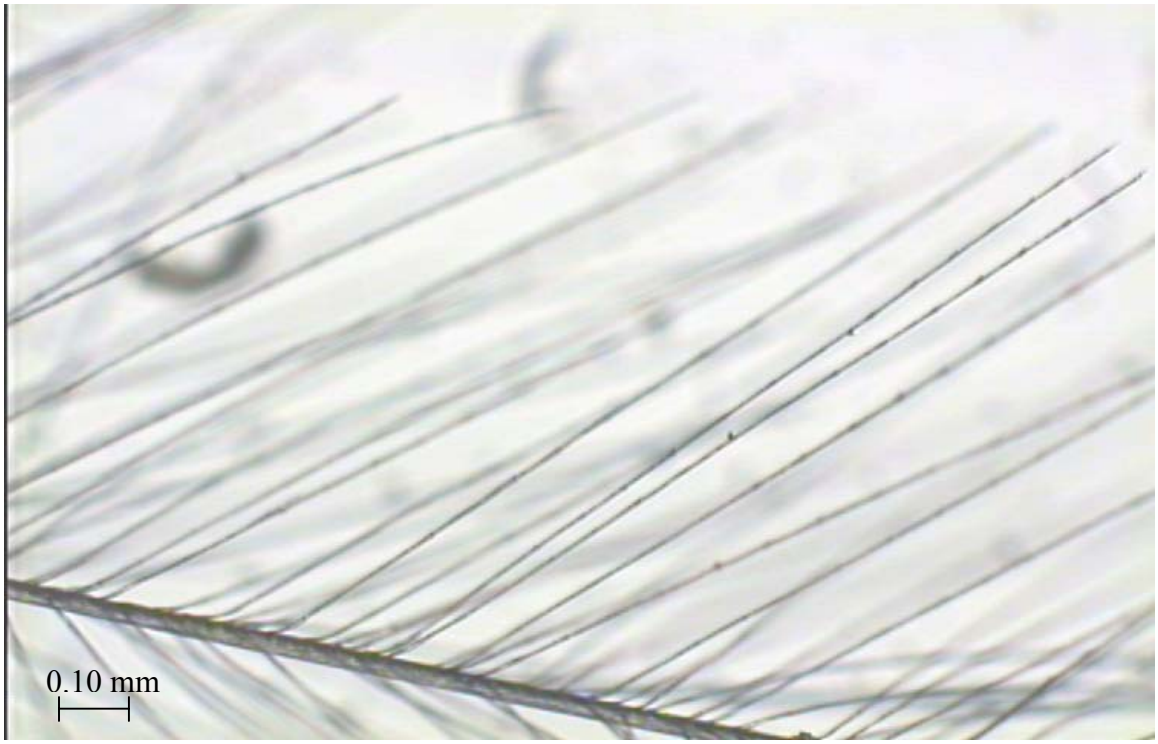

Figure 2.3.6(A) Secondary arms before deformation.

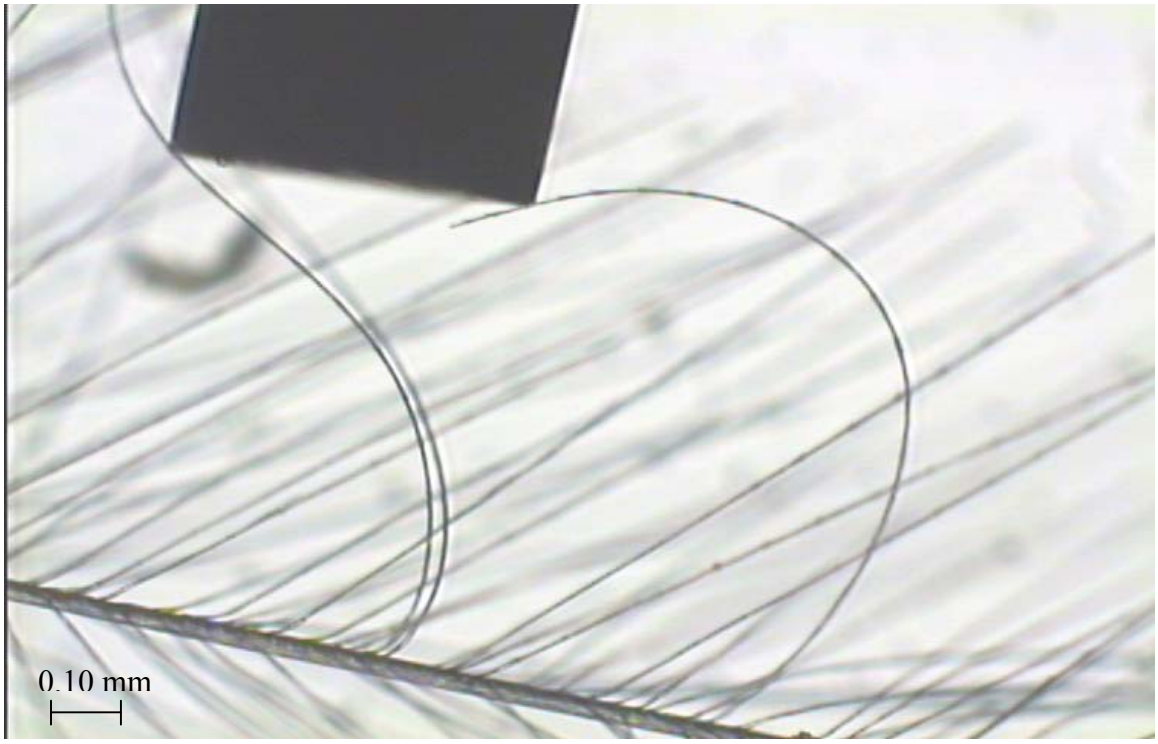

Figure 2.3.6(B) Secondary arms in deformed state.

Figure 2.3.6(C) Secondary arms post deformation, returned to original position.

The ability of these secondary structures to store elastic energy and "spring-back" contributes to the resilience of down. In order to further explore the exact influences of these different structures, the dynamics of the down mass will be studied under the microscope as well.

2.4 Dynamic Microscope Work

In order to observe the deformation mechanisms in situ, a series of photos were taken in short succession under a displacement controlled loading condition. A "flip-book" movie was then constructed from these images using Microsoft MovieMaker 2 software. A device was built to incrementally compress a goose down sample while being viewed under the same microscope used in the static studies above.

The setup (Figure 2.4.1) consists of a 1.5 millimeter thick mild steel "U" shaped track sandwiched between two pieces of Plexiglas. A metal slide moves in the track in order to compress the goose down. A precision drafting compass was to incrementally move the slide. It was necessary to keep the space between the pieces of Plexiglas small in order to keep structures in the focal plane throughout deformation.

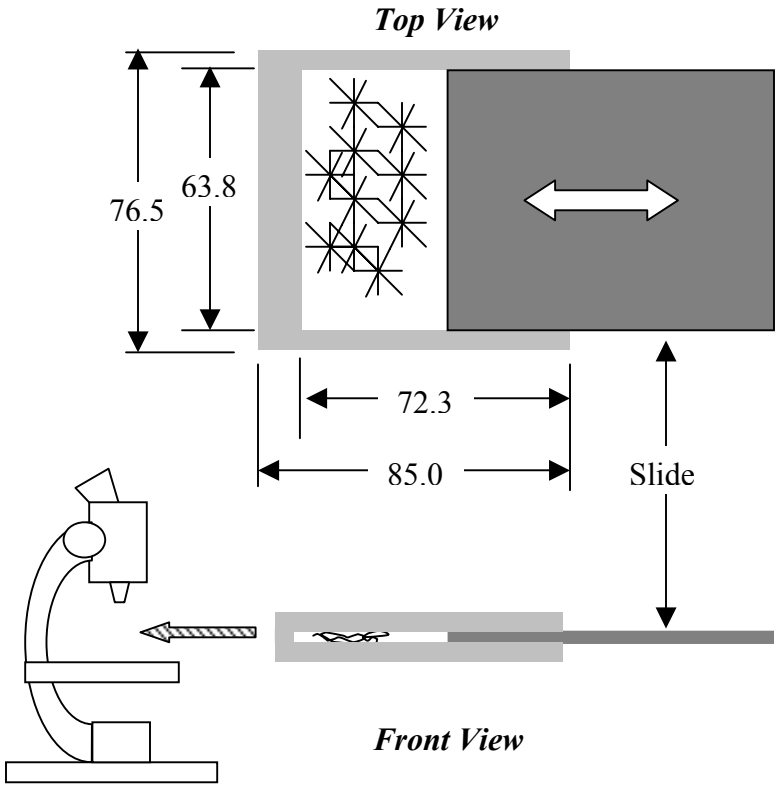

Figure 2.4.1 Schematic of test set-up used for dynamics studies. Dimensions in millimeters.

These studies illustrated several events that help to explain the compression-recovery behavior of goose down. The tertiary structures were seen to cause a single secondary to be bent at multiple locations and store more elastic energy. Furthermore, the tertiary structures prevent the secondary structures from slipping and cause the

secondary structures to undergo even greater bending. Both of these effects are significant in allowing goose and duck down to store more elastic energy than wool and synthetic polymer materials composed of smooth filaments. Generally, two secondary structures will slide freely on one another until two tertiary structures meet, and then bending commences. Typically the tertiary-to-tertiary unions will slip past one another once a certain degree of relative displacement between primary structures has occurred. At lower densities, more relative translation was observed within the goose down. As compression continues an increasing number of secondaries remain bent due to fewer tertiary-to-tertiary engagements slipping. The stored elastic energy in these deformed secondaries is significant and is responsible for the recovery.

The inability of secondary structures to slip results in re-orientation of the primary structures perpendicular to the loading direction (Figure 2.4.2). The preferential orientation of fibers in this manner is commonly acknowledged in the literature discussing random-fiber networks. (Komori *et al.*1991,1992 , Lee *et al.* 1989,1992A/B) As the density increases and the primary structures become more oriented, the contacts become more stable and increase at a greater rate.

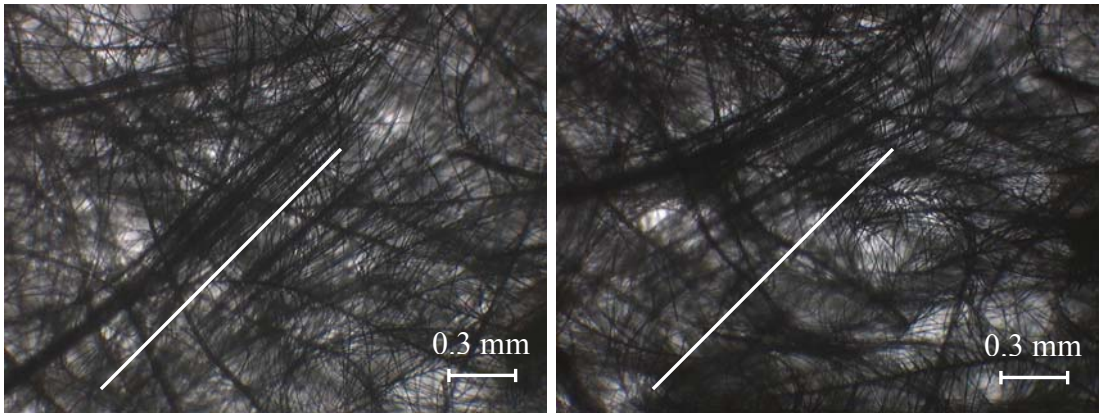

(a) (b)

Figure 2.4.2 Change in orientation before (a) and after (b) an applied displacement in the vertical direction.

Three different grades of goose down were studied. Two samples had fill power ratings of 500 and 600, while the third was a premium sample that was 92% down clusters. Based on Figure 2.1.1, this premium sample would have a fill power over 700. Surprisingly, a significant difference in cluster size was not observed between the three grades; however, there was an appreciable difference in the quantity of feathers and loose primary structures. The presence of feathers is significant because under high compression they have a tendency to trap the primary structures and cause permanent entanglements. Unlike the pinning that occurs due to the tertiary structures, the primary and secondary structures caught in feathers do not free themselves, even when the system is perturbed in an attempt to redistribute the primaries. Furthermore, feathers are two-dimensional structures and will only support restoration in two directions, whereas the down clusters exhibit a three-dimensional structure.

2.5 Material Properties of Down

Very little work has been published regarding the physical behavior of down as a bulk material or the individual clusters and their structures. Some work has been done by Bonser (1999, 2001) to determine the modulus of the Beta-Keratin that makes up most feathers, including down. Bonser specifically tested the modulus of a single primary branch of commercially treated goose down and determined a Young's modulus of 1.31 GPa, while duck down had a modulus of 2.21 GPa. The disparity between the two moduli is interesting and somewhat unexpected. As pointed out by Bonser (2001), the hydration of the down could contribute to this discrepancy. Another explanation could be an inherent difference in the crystal structure of the Beta-Keratin.

The manner in which the primary and secondary structures behave suggests that they may have a different crystalline structure. The secondaries exhibit a somewhat stiff, highly elastic response while the primaries are much stiffer. Due to these observable differences, the secondaries appear to be where most of the reversible deformation takes place; as well as storing elastic strain-energy. Any model focusing on the bending of these secondaries needs to account for the bending rigidity of these structures; however, the small size poses numerous problems for determining the bending modulus.

One possible method to determine the bending rigidity of a single secondary would be a three-point bend test. The secondary can be suspended across a piece of cardstock while a very light weight is placed in the middle of the fiber. The deflection of the fiber can be measured using a microscope and image analysis. With the deflection and applied load known, the bending rigidity can be determined from simple beam theory. A benefit of this method is that the bending rigidity can be determined as a whole

and it is not necessary to calculate the moment of inertia independently. The moment of inertia for a round fiber depends on the radius of the fiber, r_f, raised to the 4th power which compounds any errors made in measuring r_f.

2.6 Physics of Down Deformation

The Dupont Corporation tested cyclic compressive behavior of goose down in a piston-cylinder device for five cycles as shown in Figure 2.6.1.

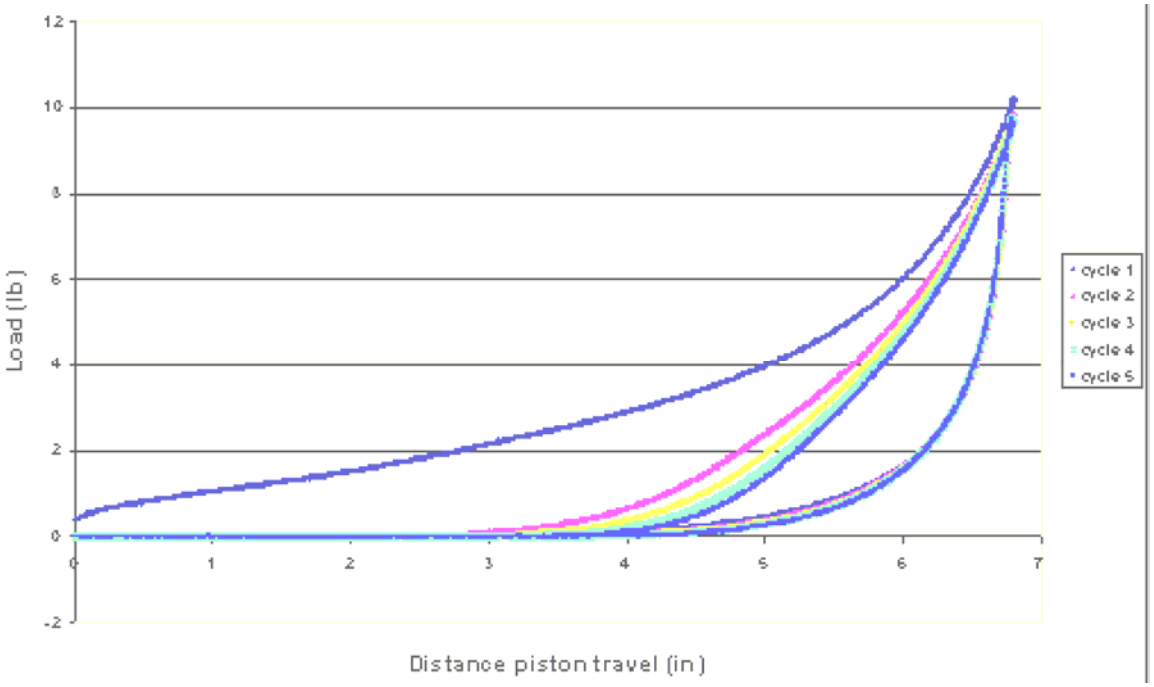

Figure 2.6.1 Force-displacement curves for cyclic compression of goose down in a piston-cylinder device. Courtesy of Dupont Corp.

The device was designed with small holes strategically drilled into the walls of the cylinder in order to allow air to escape during compression and re-enter during the recovery. Several key observations can be made relating the behavior shown in Figure

2.6.1 to the goose down morphology. The results from these explorations will be used to inspire relationships that can be implemented into the model developed in Chapter IV.

The different behavior of the initial loading curve from the unloading and reloading curves is due to several reasons. First, the piston and cylinder may have made contact during the first cycle that could have caused a response due to friction between the cylinder wall and piston in addition to the reaction of the goose down. This effect, if present, most likely corrected itself in the subsequent loading cycles. More importantly, based on the dynamic observations discussed above, the primary structures undergo irreversible reorientation and translation. These changes in the internal structure are the primary reason for the different loading behaviors. The degree of translation and reorientation that occurs most likely depends in large part on the initial density of the mass. A less dense sample will have fewer interactions to drive the re-orientation; however, the probability of a rotating primary encountering another structure that might inhibit it from fully rotating is lower for a sparser material.

Any initial compaction will influence the overall behavior of the bulk. In the experiment described previously, there was little to no initial compression of the mass. In subsequent cycles to the same peak load, the primary structure orientation distribution will undergo some reversible changes while the secondary structures allow for the majority of the deformation. Therefore, most of the permanent deformation (residual deformation upon removal of compressive load) is due to the permanent change of the orientation distribution of the primary structures.

The observed hysteresis in the loading and unloading paths is due to energy expended in re-orienting and translating the primary structures. The tertiary structures are

shaped as “hooks” and will only prevent slipping in one direction along the secondary and remain in contact only when pressed together. In the absence of forward compressive load engaging the tertiary contacts, they will rapidly lose contact. Therefore, as soon as the compressive load is relaxed, tertiary engagements will disengage very quickly, resulting in the sharp drop in the unloading branches of the force-displacement curves show in Figure 2.6.1. This is comparable to a phase transition during unloading, akin to reversible martensitic transformation in shape memory alloys for example.

The sharp upturn near the end of the compression is likely due to a combination of orientation and density effects. The density of tertiary contacts has increased and the orientation distribution of the primary structures has also evolved so that more stable contacts form at a higher rate, resulting in a stiffer response.

CHAPTER III

EXISTING MODEL FRAMEWORKS

Currently, there are no constitutive models that specifically address the behavior of goose down so a number of different frameworks applicable to the behavior of goose down have been reviewed. The models that have been developed for hyperelastic materials and textile random fiber networks have some relevance to the goose down problem. The term "random fiber network" is generally used to describe materials throughout textile studies that consist of an *initially* random distribution of fibers. Wool, some papers, yarns, and felts are materials commonly studied within the context of random fiber networks. Some of these materials are also called nonwovens, implying that they are only "held" together by the natural random interlocking of the fibers or weak bonding in the case of paper. While wool and synthetic fibers typically considered in most random fiber network models are smooth, the loose arrangement of fibers is somewhat similar to that of goose down and may limit the applicability of these models.

Constitutive models have also been developed do describe hyperelastic, or rubber-like, materials. The force-displacement relationship of the piston-cylinder experiment presented in Figure 2.6.1 exhibits some similarity to the observed response of rubbers and justifies further inspection of these models. Furthermore, a polymer can be thought of as a network of molecular chains that interact with each other to influence the overall behavior of the material, which may be analogous to the internal interactions of goose down. The constitutive models for hyperelastic materials have also been developed within the context of continuum which allows them to be formulated much easier than the

micromechanics intensive models that attempt to capture the behavior of random fiber networks.

3.1 Random Fiber Network Models

The common starting point for all studies of random fiber networks is van Wyk's (1946) model for the compression of wool. He determined the following linear relationship between the applied pressure, $\overline{P}$, and change of the cube of the inverse volume, i.e.,

$$\overline{P} = \frac{KE_f m_f^{\,3}}{36\rho_f^{\,3}}\left(\frac{1}{V^3} - \frac{1}{V_0^3}\right) \tag{3.1}$$

where K is a constant based on characteristics of the fiber mass that can be determined experimentally *if* the Young's modulus of a fiber, E_f, is known. The total mass of the fibers is m_f, and V_0 is equivalent to the volume of the wool mass at zero pressure, and ρ_f is the density of the fiber material.

In developing his theory, Van Wyk simplified the problem to one of only beam bending, neglecting the effects of orientation, slippage, and crimp. Crimp is a measure of the natural curvature of a fiber and can influence the bulk properties of a fiber mass. (Dunlop 1983) Slippage from this point on refers to the frictional sliding that occurs between the fibers. A bending element in the van Wyk model is determined by the length of fiber found between two adjacent contact points. Therefore, the equation for a beam

with fixed ends was used to determine the relationship between the force, F_c, applied between the contacts and the resulting displacement, δ:

$$F_c = \frac{24 I_f E_f}{b_f^{\,3}} \delta \tag{3.2}$$

Here I_f is the moment of inertia of the fiber and E_f is the Young's modulus of a single fiber, and b_f is the element length based on the fiber packing density. Van Wyk assumed that the contacts were equally spaced along the length of a fiber. With this assumption, the total number of contacts can be determined for a specific b_f when the total length of fibers in the system is known.

While van Wyk does not include friction in his model, he does acknowledge that it likely plays a role in the observed hysteresis, and suggests that other factors are likely to be responsible as well. He also pointed out that under cyclic compression the response curves for wool shift for several cycles and then the system stabilizes, a behavior also observed by Beil *et al.* (2002A/B) and Dunlop (1983).

Dunlop (1974, 1979, 1981, 1983) conducted several experiments with a piston-cylinder device (1974) and acoustic emission equipment (1979, 1981) to study the compressive behavior of wool fiber assemblies. The piston-cylinder experiments yielded a nonlinear relationship between the inverse volume cubed and applied pressure, which does not agree with the linear relationship derived by van Wyk. These experiments also showed that irreversible deformation accompanied by hysteresis occurs during cyclic deformation of a wool mass, a behavior also observed in goose down. These studies also allowed Dunlop to conclude that constant K in van Wyk's model is not independent of

the V_o or the initial fiber density within the mass. Dunlop also observed that determining any model constants from experiments with these materials is extremely difficult because the behavior depends heavily on the configuration of the fibers where consistency is difficult to maintain. Dunlop suggested that all samples should be exposed to the same cyclic loading until all irreversible behavior ceases before any measurement of model parameters is completed.

Dunlop (1979) used acoustic emission equipment to record the acoustic output of a wool fiber mass undergoing cyclic compression. Dunlop found that the total amount of acoustic emission steadily decreased with each cycle. The source of the acoustic emission was attributed to the frictional sliding of the fibers during compression. The decrease in overall emission with cycles suggests that the amount of slippage decreases with each cycle.

Dunlop (1981) also used acoustic emission equipment to study the dynamic bulk modulus of wool samples. Based upon the van Wyk theory, the dynamic bulk modulus may be defined in terms of a constant, k_d and bulk density ρ, i.e.,

$$K_d = \frac{KE_f}{12\rho_f^3}\rho^3 \tag{3.3}$$

Dunlop found that the bulk modulus linearly increased with the *cube* of the bulk density which agrees with the expression for the bulk modulus derived from the van Wyk theory. The constant K in the van Wyk theory may be evaluated from experimentally determined values of K_d. The values for K determined from Dunlop's experiments did not necessarily match the values of K suggested by van Wyk for modeling the experimental

data. It is likely that these differences arise partly from K being assumed constant throughout the deformation while in reality it is based on material characteristics that evolve with deformation. Dunlop suggested that the constant bending element length proposed in the van Wyk theory may also contribute to the difference in the values of K determined from the model and experiment. Dunlop implemented a distribution of bending element lengths into the van Wyk theory and found that the modified theory could "comfortably" account for the difference in K values.

Dunlop (1983) introduced three rheological models to capture the essence of the hysteresis and irreversible deformation that he observed in his experimental works. The most successful model (Figure 3.1.1) incorporated a series of elements composed of a nonlinear spring and block sliding on a surface with Coulomb friction. A slightly different series model was also considered, but did not capture the hysteresis effect as smoothly, although it did do a better job of capturing the irreversible deformation that occurs during the first cycle. While these models did capture the essence of the material behavior they did not directly related to specific material properties.

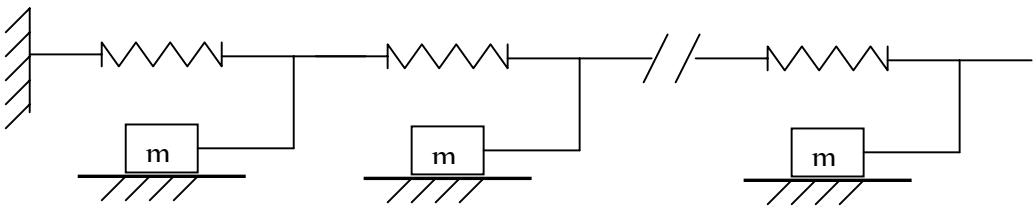

Figure 3.1.1 Rheological model used by Dunlop (1983) to capture hysteresis.

Komori *et al.* (1977,1978,1991A/B) were among the first to explore the detailed micromechanics of fiber assemblies. They worked to develop mathematical models that incorporate length and orientation effects through the use of distribution functions. The

expressions and methodology for determining these relations is extremely complicated and ambiguous. Furthermore, a direct application of the specific equations to goose down is not necessarily obvious due to the inherently different structure of the two materials. For these reasons, only the general concepts, which do have relevance to goose down, will be presented here. Komori and Makishima (1977, 1978) first determined an expression for the number of fiber-to-fiber contacts dependent on a fiber orientation distribution function (FODF) and a fiber length distribution functions (FLDF).

Determining the number of contacts is of fundamental importance since the primary energy mechanisms, slipping and bending, are related to the nature and quantity of the contacts. The probability that a fiber lies within a certain orientation, defined by the polar angle, θ, and azimuthal angle, ϕ, (Figure 3.1.2), is found by integrating the FODF over a solid angle defined by $\sin\theta d\theta d\phi$. The FODF, $\Omega(\theta,\phi)$, must satisfy the following normalization condition when integrated over all possible orientations:

$$\int_0^{2\pi} d\theta \int_0^{2\pi} d\phi \Omega(\theta,\phi)\sin\theta = 1 \tag{3.4}$$

Eq. 3.4 can be interpreted as the probability of finding a fiber within the range of all possible orientations, which must be one.

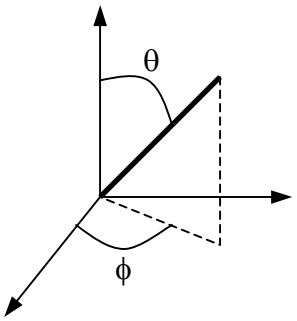

Figure 3.1.2 Measurement of polar (θ) and azimuthal (ϕ) angles.

Unfortunately, it is difficult to determine the actual FODF in practice and leads to the common assumption that the fibers are randomly oriented, meaning every orientation is equally likely and FODF is a constant determined through the constraint imposed by Eq. 3.4. The constant value may vary depending different symmetry conditions that may be assumed. If the FODF is symmetric about both θ and ϕ the normalization condition yields a constant FODF equal to $1/(2\pi)$. If distribution or orientations is not symmetric in the plane where ϕ is measured, then the limits of integration for ϕ in Eq.3.4 become 0 and 2π and the FODF has a constant value of $1/4\pi$.

For a general distribution of fiber orientations, Komori *et al.* determined that the average number of contacts per unit volume, $\overline{n}_v$, is given in terms of the fiber diameter D_f, total fiber length in the volume, L_f, and orientation, and orientation related function I_o.

$$\overline{n}_v = D_f L_f^2 I_o \tag{3.5}$$

where I_o is an orientation related factor, i.e.,

$$I_o = \int_0^{\pi} d\theta \int_0^{\pi} d\phi \int_0^{\pi} d\theta' \int_0^{\pi} d\phi' (\sin\chi)\mathbf{\Omega}(\theta,\phi)\mathbf{\Omega}(\theta',\phi')\sin\theta\sin\theta' \qquad (3.6)$$

The angle χ is the angle formed between the fiber with orientation ϕ' and θ' and the fiber defined by the angles ϕ and θ. The functional forms of the expressions in the equations above are not easily determined and would require significant experimental effort determine accurately.

Carnaby and Pan (1989) and Komori *et al.* (1991A) have extended the ideas of Komori *et al.* (1977) to micromechanics models that incorporate slip (Carnaby *et al.* 1989) and orientation change (Komori *et al* 1991A) to the overall behavior of an elemental volume of fibers. Through the inclusion of fiber slippage, Carnaby *et al*.(1989) were able to predict the qualitative aspect of the hysteresis and made the important observation that not all of the orientation changes are reversible due to friction preventing fibers from returning to their original orientation. Therefore, the slip during the recovery stage is as important, if not more so, than the slip that occurs during compression in influencing the amount of irreversibility.

Carnaby *et al.* derived a slip condition by resolving net contact force in the *j* direction, C_j, into components normal, C_{jn}, and parallel, C_{jp}, to the fiber axis as shown in Figure 3.1.3. They assumed a consistent contact force among all contacts and defined the frictional force parallel to the fiber axis, C_f as

$$C_f = \mu_{fr} C_{3n} + WF_o b_f \qquad (3.7)$$

Here, WF_0b_f is called the *withdrawal* force and represents the force resisting slippage when there is no applied pressure on the fiber network and μ_{fr} is the static coefficient of friction between the fibers. The fiber bending element length, b_f is the mean fiber length which is dependent on the orientation factor, I_o.

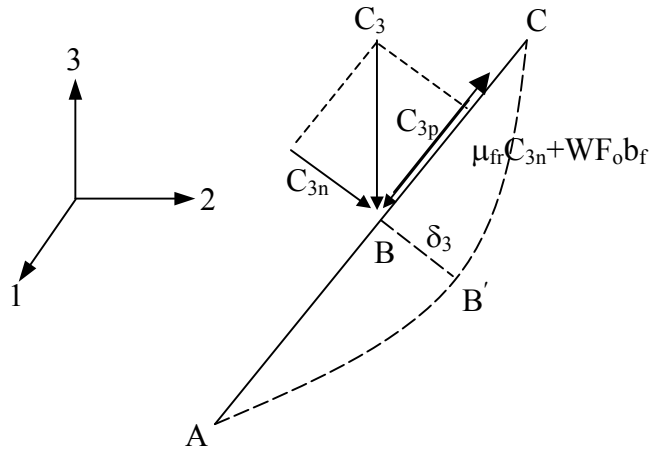

Figure 3.1.3 Carnaby *et al.* (1989) representation for fiber-to-fiber contact.

Based on Figure 3.1.3, the slip condition developed by Carnaby *et al.* can be determined from a force balance along the direction parallel to the undeformed fiber axis. Therefore, slip will occur when the following condition is met

$$C_{jp} \geq \mu_{fr} Cjn + WF_0 b_f \qquad (3.8)$$

Carnaby *et al*. postulated that the external stress of the mass is distributed through the contacts. A thin section cut through the fiber assembly normal to the loading direction *j* will intersect few, if any contacts, denoted by n_{bj}. The proportion of slipping contacts is denoted by *SN* and the fraction of non-slipping contacts follows as (*1-SN*).

Based on these assumptions, they determined an expression relating the externally applied pressure of the system, $\overline{P}_j$, slipping contact force, C_{sj}, and non-slipping contact force C_j

$$\overline{P}_j = (SN)n_{bj}C_{sj} + (1-SN)n_{bj}C_j \tag{3.9}$$

In formulating their theory, Carnaby *et al.* (1989) assumed that all fibers were identical and linear elastic in bending and neglected components associated with torsion, compression, and extension. They also assumed that no new contact points are created during an incremental increase in load. Also, they assume that all fibers within the network displace in unison with the overall deformation of the fiber network. This assumption is also referred to as the *affine* assumption.

Carnaby *et al.* suggested that the stress and strain of the unit fibrous cell are related through the tangent compliance matrix, $\mathbf{S}_T$, i.e.,

$$\Delta\boldsymbol{\varepsilon} = [\mathbf{S}_T(\mathbf{P}_0, \boldsymbol{\varepsilon}_0)]\Delta\mathbf{P} \tag{3.10}$$

Assuming that the cross-sectional area, A_j, defined normal to the direction j of the applied pressure $\overline{P}_j$ remains constant, the diagonal components of $\mathbf{S}_T$ are expressed as

$$\frac{1}{S_{T_{jj}}} = \frac{-\Delta\overline{P}_j / A_j}{\Delta\varepsilon_j} \tag{3.11}$$

Carnaby *et al.* propose that the representative cross sectional slice, of height b_j, will deform by a thickness of δ_{jj}, resulting in a change in the uniaxial strain defined by

$$\Delta\varepsilon_j = \frac{\Delta\delta_{jj}}{b_j} \tag{3.12}$$

Carnaby *et al.* determined the deflection of a fiber between two contact points based on the simple beam theory for a beam fixed at both ends with flexural rigidity B_f, *i.e.,*

$$B_f = E_f I_f = \frac{E_f \eta_f \pi D_f^{\,4}}{64} \tag{3.13}$$

The Young's modulus, E_f, and fiber diameter, D_f, are the same here as in the van Wyk model and η_f is a shape parameter related to the fiber cross-sectional shape. After simplification and substitutions, Carnaby *et al.* determine expressions for the diagonal components of the tangent compliance matrix in compression as

$$E_{T_{jj}} = \frac{192}{\pi^2} E_f \eta_f V^3 \frac{K_j^2 I_j^2}{m_{jj}} \left(1 - SN + SN \frac{\Delta C_{sj}}{\Delta C_j} \right) \tag{3.14}$$

and recovery as

$$E_{T_{jj}} = \frac{192}{\pi^2} E_f \eta_f V^3 \frac{K_j^2 I_j^2}{m_{jj}} \left(1 - SN - SN \frac{\Delta C_{sj}}{\Delta C_j} \right) \tag{3.15}$$

Here, K_j, I_j, and m_{jj} are complex functions based on integration over the FODF based on the work of Komori and Makishima (1978).

This model captures the hysteresis and continued reduction in resistance to compression with successive cycles. It also captured some of the irreversibility observed experimentally. Carnaby *et al.* noted that the lack of viscoelastic effects in the model is the likely reason for the hysteresis loop being narrower than those observed in the experimental data. The model overestimates the modulus of the mass. The Poisson's ratio was also determined from the tangent compliance terms and was found to increase from 0.3 to a maximum value of 0.7 and then decreases to 0 at the maximum compression. The values near zero are expected while the values greater than 0.5 do not make sense since that suggests the volume *increases* with compression.

A similar approach was taken by Komori and Itoh (1991A); however, they argued that the dependence between fiber direction and orientation is important and should be included. They claimed that neglecting this detail affects how orientation plays a role in the development of the fiber-to-fiber contacts and in turn the overall behavior of the material. In order to implement their hypothesis into their model, Komori and Itoh (1991A) defined a bending element length that was depended upon the FODF.

Komori and Itoh (1991A) derived the following relationships for the change in polar and azimuthal angles as a function of the applied normal strains, respectively:

$$\theta^* - \theta = \sin\theta\cos\theta(\cos^2\phi\delta\varepsilon_{11} + \sin^2\phi\delta\varepsilon_{22} - \delta\varepsilon_{33})$$

$$\phi^* - \phi = -\sin\phi\cos\phi(\delta\varepsilon_{11} - \delta\varepsilon_{22}) \qquad (3.16)$$

As with the models of Carnaby and Lee discussed above, the azimuthal angle is independent of strains applied in the 3-direction. For uniaxial, laterally confined compression ($\delta\varepsilon_{11} = \delta\varepsilon_{22} = 0$) in the 3-direction these equations simplify to:

$$\theta^* - \theta = \sin\theta\cos\theta(-\delta\varepsilon_{33})$$

$$\phi^* - \phi = 0 \qquad (3.17)$$

Komori and Itoh (1991A) determined the total increment in the strain-energy density of based on the incremental change in normal strain

$$\delta\Psi = 32 B_f D_f^2 L_f{}^3 \int \left[J(\underline{\varepsilon};\mathbf{o})\right]^2 \left[\sum_i \mathbf{o}_i^2 \delta\varepsilon_{ii}\right]^2 \Omega(\underline{\varepsilon};\mathbf{o}) d\omega^\circ \qquad (3.18)$$

As before, L_f is the total length of fiber per unit volume of the assembly. The integration takes place over all orientations defined by the solid angle ω°. The vectors $\mathbf{o}_i$ represent the components of the fiber in the *1*, *2*, and *3* directions determined from the direction cosines and $J(\boldsymbol{\varepsilon},\boldsymbol{o})$ is a function related to the FODF derived by Komori and Makishima (1977). The stress was then determined by differentiating the incremental change in energy with respect to the incremental change in strain.

Komori and Itoh evaluated their theory for isotropic compression, laterally confined compression, and simple compression. For isotropic compression, they found their model to be equivalent to the theory of van Wyk (1946) in which case the FODF

remained constant and did not change. In the second case, the FODF transitioned from a smooth curve representing a random distribution of orientations to a sharp peak at $\theta = \pi/2$, suggesting that the fibers preferentially align away from the direction of loading. Due to confinement of the fiber mass, a stress in the transverse plane might be developed. Based on their model, Komori and Itoh (1991A) found that the lateral stress may actually surpass the normal applied stress.

For simple compression with no lateral confinement, the significant lateral stress developed in the confined case vanishes, but the mass expands in the transverse directions. Considering small strains only, Komori and Itoh determined a Poisson's ratio of ¼. Substituting this value of the Poisson's ratio into the laterally confined case results in a transverse stress that does not surpass the stress in the direction of applied loading which makes more logical sense when consider experience with these materials in everyday life. Komori *et al.* (1991A) also point out that the Carnaby *et al.* (1989) model can predict a Poisson's ratio greater than ½, suggesting that compression causes and increase of volume, which does not seem appropriate. They attribute this to the slippage criteria used in the Carnaby *et al.* model.

The Komori and Itoh model (1991A) does not specifically include any beam bending equations, and therefore circumvents the discussion of which beam boundary conditions are appropriate. Komori *et al.* (1991B) evaluated their theory for applied shear strains.

Lee and Carnaby (1992 A/B) developed a theory to determine the energy developed within a wool fiber mass based on the energy stored in the fibers due to changes in curvature of the fibers as shown in Figure 3.1.4. Lee *et al*. were not

concerned with calculating the stress-strain response of the mass but rather sought to explore the influence of certain parameters on the compressional energy of the fiber mass.

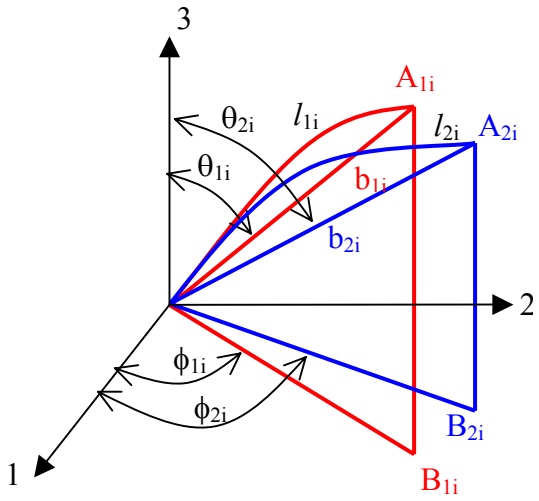

Figure 3.1.4 Fiber bending geometry for Lee *et al* (1992 A/B) model. Fiber deforms from 1 to 2.

They related the change in curvature of a fiber deformed from "1" to "2", as shown in Figure 3.1.4, to the applied external uniaxial strain through the *affine* assumption. The change in curvature was determined from the chord lengths, b_{1i} and b_{2i}, and total fiber lengths l_{1i} and l_{2i}. They established a criteria to determine if a fiber would undergo bending, straightening, or slipping. The energy for each of these deformations could then be calculated based on the fiber curvature. The total energy, Ψ, of the system equals the summation of all energy associated with the number of fibers undergoing bending, N_B, straightening, N_T, and slipping, N_S and their associated energies, E_{Bi}, E_{Ti} , and E_{Si}, respectively, i.e.,

$$\Psi = \sum_{i=1}^{N_B} E_{Bi} + \sum_{i=1}^{N_T} E_{Ti} + \sum_{i=1}^{N_s} E_{Si} \tag{3.19}$$

Lee et al. (1992B) then minimized the energy for a given applied strain and Poisson's ratio in order to explore the effect of certain parameters on the developed compressional energy. Since the Lee *et al.* model is based on the relative change in curvature, the effect of initial curvature, or crimp, of the fibers could be considered to determine the effect of crimp. They found that fibers with increased crimp resulted in a bulkier mass that required greater energy to compress. Likewise, an increase in fiber density resulted in a higher required compressional energy. They also found that the elastic energy tended to decrease with fiber diameter, but stated that further bivariate studies were necessary to determined more meaningful correlations between fiber mass properties and the bulk behavior.

Recently, Beil and Roberts (2002A/B) have used high performance computing to evaluate a finite element model for a wool fiber assembly. They modeled each individual fiber within a representative volume element (RVE). Because every individual fiber is modeled, factors such as crimp, orientation, fiber length, and slippage are automatically accounted for without having to assume any statistical distributions. In fact, this type of model on a small scale may be a viable way to explore the precise behavior of the distributions assumed in the micromechanics models.

Beil *et al.* (2002A) found that in compression the number of contacts increased at a much greater rate than that predicted in the van Wyk model. Beil and Roberts point to the absence of relative fiber motion in the van Wyk model for the discrepancy in the number of contacts. They also found that the contact forces varied widely in magnitude

which contrasts with the assumption made by Carnaby *et al*.(1989) that all of the contact forces are equivalent. In the Beil *et al.* (2002A/B) model fewer than 15% of contacts are non-slipping at any point during the compression. This observation suggests that the majority of the contacts are weak. It is very likely that the number of non-slipping contacts in goose down is far greater due to the tertiary structures opposing slippage rather than only friction.

They also found that the FODF did not change as dramatically as predicted by the Komori and Itoh (1991A) model which predicted a large degree of fiber alignment in the plane orthogonal to loading. Beil *et al.* (2002A/B) noted that the lack of alignment in the deformed material could be due, in part, to the applied boundary conditions on the RVE. This model did capture many of the complex behaviors of fiber assemblies during repeated compression-recovery cycles. A hysteresis and gradual shifting of the curves was captured. The irreversible aspects of the fiber assembly behavior were also captured.

Models have also been developed to describe the behavior of papers. (Cox 1952, Ostoja-Starzewski *et al.* (1999, 2000) Papers are essentially planar random fiber networks similar to the wool fiber assemblies discussed above. One important difference is that the fibers in paper are bonded together which changes the micromechanics involved and limits their applicability to goose down. It is worth briefly mentioning the concept of a *flocculation*, or *floc*, parameter used by Ostoja-Starzewski *et al.* (1999, 2000). The floc parameter describes the degree of clustering occurring within the material and could have implications in a later model for goose down in which spatial variations are considered. Another factor limiting the applicability of paper models is

that they usually focus on tensile behaviors while we are primarily interested in the compressive behavior of goose down.

3.2 Polymer Models

3.2.1 Hyperelastic Finite Elasticity Theory

The constitutive theory for a class of materials known as hyperelastic, or Green-elastic, may also provide a useful framework for the development of a goose down model. The constitutive framework for these materials has been used extensively for the description of rubber-like materials which are of interest because of the similarities observed in some rubbery materials and that of goose down. Malvern (1969) and Holzapfel (2000) provide excellent and thorough overviews of the hyperelastic theory beyond what is provided here.

A Green-elastic, or hyperelastic material, is a material for which a strain-energy function, $\Psi(\mathbf{F})$, exists. The strain-energy function depends upon $\mathbf{F}$, the deformation gradient and is defined per unit reference volume. The strain energy function must be defined within the following constraints:

$$\Psi(\mathbf{I}) = 0$$

$$\Psi(\mathbf{F}) \geq 0$$

$$\Psi(\mathbf{F}) = \Psi(\mathbf{QF}) \tag{3.20}$$

The first constraint requires that the strain-energy vanishes when no deformation is applied, i.e. $\mathbf{F}=\mathbf{I}$, where $\mathbf{I}$ is the identity tensor. The second constraint requires that the

strain-energy increase with deformation. The third constraint ensures that the strain-energy function is *objective* and is independent of translation and rotation. In the third constraint, **Q** is any orthogonal tensor. Through the third constraint it follows that the strain-energy function can also be defined in terms of the right-stretch tensor **U** since **F=RU** and **R** is an orthogonal rotation tensor. It then follows that $\Psi(\mathbf{F}) = \Psi(\mathbf{U})$ which also implies that Ψ only depends upon the stretching portion of **F**.

Likewise, the strain-energy function can also be derived in terms of the left and right Cauchy-Green deformation tensors, denoted **b** and **C**, respectively. These deformation tensors are related to the deformation gradient.

$$\mathbf{b}=\mathbf{F}\mathbf{F}^{\mathrm{T}}$$
$$\mathbf{C}=\mathbf{F}^{\mathrm{T}}\mathbf{F} \tag{3.21}$$

The strain-energy function can further be defined in terms of the principal invariants of **C** and **b**, i.e.,

$$\Psi = \Psi(I_1(\mathbf{C}), I_2(\mathbf{C}), I_3(\mathbf{C})) = \Psi(I_1(\mathbf{b}), I_2(\mathbf{b}), I_3(\mathbf{b})) \tag{3.22}$$

Furthermore, since the eigenvalues of **C** and **b** are the equivalent, so are their invariants.

$$I_1(\mathbf{b}) = tr(\mathbf{b}) = \lambda_1^2 + \lambda_2^2 + \lambda_3^2$$
$$I_2(\mathbf{b}) = \lambda_1^2\lambda_2^2 + \lambda_1^2\lambda_3^2 + \lambda_2^2\lambda_3^2$$
$$I_3(\mathbf{b}) = \det\mathbf{b} = \lambda_1^2\lambda_2^2\lambda_3^2 \tag{3.23}$$

The eigenvalues of **C, b,** and **U** are all related to the principal stretches, λ_i. The principal stretches are equal to the eigenvalues of the right-stretch tensor, **U**, and the eigenvalues of **C** and **b** are equal to the squares of the principal stretches. Therefore, the strain-energy can also be expressed as a function of the principal stretches.

The non-symmetric nominal stress (first Piola-Kirchhoff stress) in a hyperelastic material can be determined from the strain-energy function through the relation

$$\mathbf{P} = \frac{\partial \Psi(\mathbf{F})}{\partial \mathbf{F}} \tag{3.24}$$

The Cauchy stress, **T,** can be determined in terms of **P**, i.e.,

$$\mathbf{T} = J^{-1}\mathbf{F}\left(\frac{\partial \Psi(\mathbf{F})}{\partial \mathbf{F}}\right)^{T} \tag{3.25}$$

where J is the Jacobian and is equal to the determinant of **F**.

3.2.2 Phenomenological Rubber Elasticity Models

The hyperelastic constitutive framework outlined above has been used extensively in the description of rubber-like materials undergoing finite deformations. The Mooney, Mooney-Rivlin, and Ogden models are examples of purely phenomenological models that have been developed to describe the stress-strain relationship for incompressible

rubbers. These models define a strain-energy function which can then be used to determine the resulting stresses in the material. These models are purely phenomenological, which means that they are based on mathematical reasoning more than the molecular or structural physics that influence the material behavior. They do successfully capture the experimentally observed behavior in some circumstances.

Mooney (1940) developed one of the first models for the finite elastic deformations of rubber. Mooney's strain-energy function was developed assuming that the material is incompressible, initially isotropic, and that the shear stress is proportional to the shear strain. The Mooney strain-energy function can be defined in terms of the principal stretches, λ_i and two material constants C_1 and C_2, i.e.,

$$\Psi(\lambda_i) = \frac{C_1}{4}\sum_{i=1}^{3}\left(\lambda_i - \frac{1}{\lambda_i}\right)^2 + \frac{C_2}{4}\sum_{i=1}^{3}\left(\lambda_i^2 - \frac{1}{\lambda_i^2}\right)^2 \tag{3.26}$$

The assumption of proportionality of the shear stress and strain limits the applicability of the Mooney theory to only moderately large strains. Furthermore, the values for the constants C_1 and C_2 differ depending on whether the model is being fit for compression or tension.

Rivlin (1948) expanded upon the Mooney model by reasoning that Ψ should be symmetric with respect to the principal stretches and that the strain-energy function should also be unaltered by a rotation of the body though 180°. Using these arguments, Rivlin determined that Ψ can only depend on even powers of the principal stretches. The three invariants given by Eq. (3.23) above are the three simplest functions of the principal

stretches that will satisfy these conditions. The isochoric assumption of incompressibility implies that the third invariant must equal unity. From this constraint, two of the principal stretches can be defined in terms of the third principal stretch and the first two invariants can be re-written. Rivlin's strain-energy function can be expressed then in terms of a series of terms based on the two remaining invariants, i.e.,

$$\Psi = \sum_{i=0,j=0}^{\infty} C_1(I_1(\mathbf{b})-3)^i + C_2(I_2(\mathbf{b})-3)^j \tag{3.27}$$

For $i = j = 1$ Rivlin's expression simplifies to the Mooney result.

Ogden (1972) derived a new expression for the strain-energy of an incompressible rubber material in terms of the principal stretches and allowed for even powers, i.e.,

$$\Psi = \Psi(\lambda_1, \lambda_2, \lambda_3) = \sum_{p=1}^{N} \frac{\mu}{\alpha_p}\left(\lambda_1^{\alpha_p} + \lambda_2^{\alpha_p} + \lambda_3^{\alpha_p} - 3\right) \tag{3.28}$$

In this model, μ is the shear modulus determined in the reference configuration based on the linear theory. The exponents, α_p, are dimensionless constants. Typically, only three terms of the Ogden model are needed to sufficiently model the behavior of most materials.

3.2.3 Polymer Network Models

The models discussed in Section 3.2.1 employed purely phenomenological expressions for the strain-energy function based on mathematical reasoning rather than the details of material deformation mechanisms. In order to more closely address the relevant mechanisms, several models have been developed to express the distribution of energy stored in a network of molecular chains. The following introductory information on polymer physics is based on the very thorough treatment of rubber elasticity presented by Treloar (1975).

The total strain energy for a network of molecular chains is determined by the summation of the entropy changes over all chains in the network. This is analogous in some ways to the manner in which the total elastic strain-energy of the fiber networks models discussed above is calculated. Once the total strain-energy of the molecular network has been determined, the stresses can be determined from the hyperelastic relations presented at the beginning of this section.

The statistical network theory for polymers is based on several fundamental assumptions (Treloar 1975). First, there are N_{ch} chains per unit volume. A chain is defined as the segment between two points where cross-links occur, which is similar to the bending element definition used in the fiber network models. A single chain contains n bonds of length l for a total length of nl. The material is assumed to be incompressible and therefore maintains a constant volume which also implies that the third invariant is always equal to unity. The *affine* assumption is also instituted so that the cross-links deform as if they were embedded in an elastic continuum. Lastly, the total entropy of the network is equal to the sum of the entropies of all the individual chains. Boltzmann determined that the entropy of a single molecular chain is proportional to the *logarithm* of

the number of configurations available to a particular chain. Considering a single chain with one end located at the origin and the other end located at (x_o, y_o, z_o) the probability density for the chain based on Gaussian statistics is related to the initial end-to-end distance, r_o, i.e.,

$$p(x,y,z) = \frac{b_G^{\,3}}{\pi^{3/2}} e^{-b_G{}^2 r_o^2} = p(r_o) \tag{3.29}$$

where,

$$r_o^2 = x_o^2 + y_o^2 + z_o^2 \tag{3.30}$$

and the entropy of a single chain is equal to

$$s = k_b \{\ln p(x,y,z) dv\} \tag{3.31}$$

The entropy for a Gaussian chain in the original state, for a constant dv, is expressed in terms of the constant b_G from the Gaussian distribution function and the Boltzmann constant k_b as

$$s_o = c - k_b b_G{}^2 (x_0^2 + y_0^2 + z_0^2) \tag{3.32}$$

The chain then undergoes a deformation equivalent to the deformation applied to the entire material as dictated through the *affine* assumption and represented by the principal

stretches, λ_i. As a result of the deformation, the chain has a new end-to-end distance, r, and the coordinates of the free end are now located at (x, y, z) with

$$x = \lambda_1 x_o \qquad y = \lambda_2 y_o \qquad z = \lambda_3 z_o \tag{3.33}$$

The entropy of the deformed Gaussian chain, s, is then given by

$$s = c - k_b b_G^2 (\lambda_1^2 x_o^2 + \lambda_2^2 y_o^2 + \lambda_3^2 z_o^2) \tag{3.34}$$

. The change in entropy of the chain due to deformation can then be expressed as

$$\Delta s = -k b_c^2 \{(\lambda_1^2 - 1)x_o^2 + (\lambda_2^2 - 1)y_o^2 + (\lambda_3^2 - 1)z_o^2\} \tag{3.35}$$

Summation of the change in entropy over all chains, N_{ch}, gives the total change in entropy, ΔS, i.e.

$$\Delta S = \sum \Delta s = -k b_G^2 \left\{(\lambda_1^2 - 1)\sum x_o^2 + (\lambda_2^2 - 1)\sum y_o^2 + (\lambda_3^2 - 1)\sum z_o^2\right\} \tag{3.36}$$

It is assumed that in the unstrained state the chains are randomly oriented and therefore have no directional preference and that the summation of all chain components in the network in each direction will be equal, i.e.

$$\sum x_o^2 = \sum y_o^2 = \sum z_o^2 \tag{3.37}$$

Where the summation in each direction is equal to the initial end-to-end distance r_o

$$\sum r_o^2 = \sum x_o^2 + \sum y_o^2 + \sum z_o^2 \tag{3.38}$$

which leads to

$$\sum x_o^2 = \sum y_o^2 = \sum z_o^2 = \frac{1}{3}\sum r_o^2 \tag{3.39}$$

The total change in entropy can then be expressed

$$\Delta S = \sum \Delta s = -\frac{1}{3} N_{ch} k_b b_G^2 \overline{r}_o^2 \left(\lambda_1^2 + \lambda_2^2 + \lambda_3^2 - 3\right) \tag{3.40}$$

where $\overline{r}_o^2$ is the mean-square end-to-end is distance of the molecular chains in the unstrained state and can be related to the constant b_G i.e.

$$\overline{r}_o^2 = \frac{3}{2b_G^2} \tag{3.41}$$

and the total change in entropy simplifies to

$$\Delta S = -\frac{1}{2} N_{ch} k_b \left(\lambda_1^2 + \lambda_2^2 + \lambda_3^2 - 3 \right) \tag{3.42}$$

The total change in entropy can be related to the corresponding change of the free energy according to

$$\Delta \Psi = -T \Delta S \tag{3.43}$$

Assuming that there is no free energy in the initial state, the free energy associated with entropic effects of chain configuration may be written as

$$\Psi(\lambda_1, \lambda_2, \lambda_3) = \frac{1}{2} N_{ch} kT (\lambda_1^2 + \lambda_2^2 + \lambda_3^2 - 3) \tag{3.44}$$

This result for the molecular network based on Gaussian chains is equivalent to the Mooney-Rivlin and Ogden phenomenological theories that were presented above. The Gaussian theory and phenomenological models discussed above fail to capture the steep upturn in the stress-strain curves obtained experimentally for rubbers in tension. The failure of these models to capture that steep upturn in tension is due to the Gaussian approximation which is only valid for chain configurations in which the end-to-end distance of the chains is significantly less than the fully extended chain length. In the stretching of a polymer, significant straightening of the molecular chains can occur, resulting in a response that stiffens considerably as more chains become fully extended.

In order to capture this dramatic stiffening at high stretches, molecular network theories have been developed based on non-Gaussian statistics. The non-Gaussian statistics allow for finite extensions of the molecular chains for values of r close R_{fe}, the fully extended chain length The probability density for the non-Gaussian chain is expressed in terms of the inverse Langevin function, L^{-1}.

$$\ln p(r) = c - n\left(\frac{r}{nl}\beta_{L^{-1}} + \ln\frac{\beta_{L^{-1}}}{\sinh\beta_{L^{-1}}}\right) \tag{3.45}$$

with $\beta_{L^{-1}}$ defined as

$$\beta_{L^{-1}} = L^{-1}\left(\frac{r}{nl}\right) \tag{3.46}$$

following from Eq. 3.31, the entropy of the non-Gaussian chain is given according to

$$s = c - k_b n\left(\frac{r}{nl}\beta_L + \frac{\beta_L}{\sinh\beta_L}\right) \tag{3.47}$$

where this expression depends on the determination of r, the current end-to-end distance of the chain.

The non-Gaussian formulation for a single chain has then been used to determine the entire network response. In order to simplify the problem, the non-Gaussian theory is usually implemented into the three-chain model by James and Guth (1943), the four chain model of Flory and Rehner (1943), or the eight-chain model of Arruda and Boyce (1993). These models simplify the overall network geometry by assuming that the network response can be approximated by the response of the representative element as shown in Figure 3.2.1.

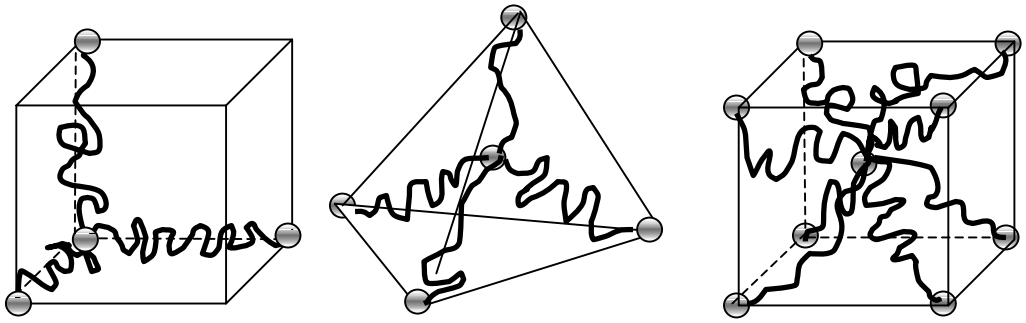

Figure 3.2.1 (A) Three-chain, (B) four-chain, and (C) eight-chain models.

The deformation applied to the element is used to determine the r based on geometric analysis due to the *affine* deformation assumption. In turn the value of r can usually be expressed a function of the principal stretches, λ_i, such that the stress change in entropy can be expressed as a function of the principal stretches which then leads to an expression for the strain-energy function in terms of the stretches. The strain-energy density function can then be differentiated with respect to the principal stretches to determine the stresses.

It should be noted that all of the molecular theories discussed to this point have focused on chains that behave according to the statistical theory. Exceptions from the statistical theory arise when the effects of chain entanglements and cross-links are included. These factors influence and complicate the theory used to determine the network response. Shepherd (2002) provides a good explanation of these complicating factors and implements them into a novel model based upon the Arruda-Boyce eight-chain network model.

3.2.4 The Mullins Effect

The Mullins effect is a well-characterized behavior of polymers and rubber-like materials. The idealized Mullins effect is a stress softening phenomenon that occurs under repeated loading conditions and was first studied in depth by Mullins and Tobin (1957). An *ideal* Mullins behavior is shown in Figure 3.2.2, taken from Ogden *et al*. (1999). Some similarities can be seen between the *ideal* Mullins effect and the behavior of goose down (Figure 2.6.1). One crucial difference is that the *ideal* Mullins behavior is perfectly elastic and does not exhibit any irreversible behavior. However, an ideal Mullins material continues to reach the same maximum stress for repeated loadings to the same deformation despite exhibiting a different path during unloading and reloading as goose down also does. These similarities suggest that a model capable of capturing the Mullins effect may also be able to capture some of the behaviors observed for goose down.

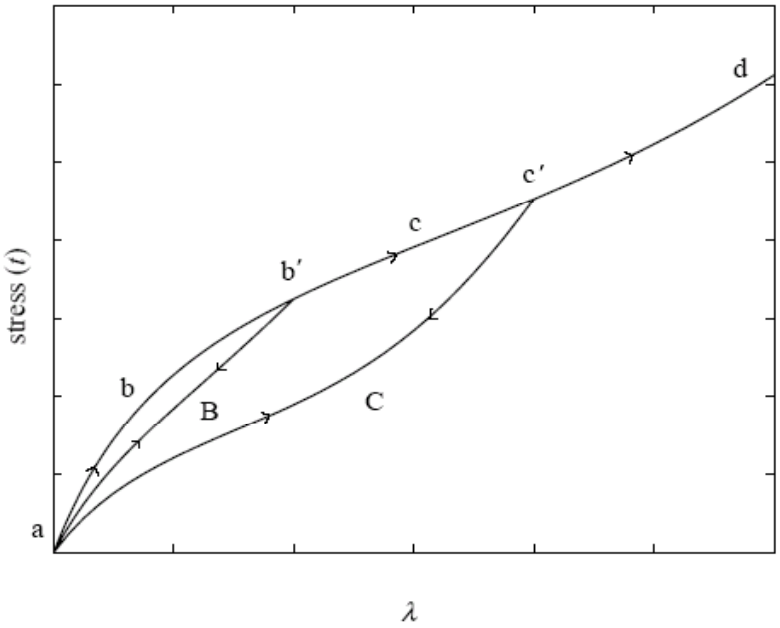

Figure 3.2.2 Representation of the behavior of an *ideal* Mullins material from Ogden *et. al* (1999).

The top response curve in Fig. 3.2.2 containing abb'cc'd is the response of the undamaged material. The paths containing B and C loading and unloading curves for a *damaged* material. A virgin material loaded along abb' and then released at point b' will follow the path b'Ba during recovery. Any reloading for the material will follow aBb' until the stretch at b' is exceeded, at which point the material reverts back to the virgin material response.

Several physical explanations for this behavior have been offered. All of these explanations are based on the idea that a physical transformation of the *internal* structure of the material is taking place. Mullins and Tobin hypothesized, in general terms, that the phenomenon was due to a deformation-induced phase transformation of the internal structure of the material. In particular, the transition of a stiff, *hard*, phase to a less stiff, *soft*, phase that results in a softer material response in subsequent cycles. Other authors

(Beatty *et al. 1993* and Marckmann *et al*. 2002) have offered more precise explanations based on the molecular chain network behavior during deformation. Beatty *et al.* (1993) associated the hard phase with chain clusters due to entanglements and chain bonding while Marckmann *et al.* (2002) attributed the transition to the presence of chain-filler and chain-link breakage.

Most theories account for stress softening by including a damage function that depends on a damage variable, $\xi \in [0,1]$, and the maximum deformation of the material. Physically, this damage variable can be related to the phase transition theory hypothesized by Mullins and Tobin.

Gurtin *et al.* (1981) introduced a theory in which the stresses during reloading and unloading are related to the peak stress, σ_{max}, at the end of the loading path through the damage function, $F(\xi, \varepsilon_{max})$, i.e.,

$$\sigma = F(\xi, \varepsilon_{\max})\sigma_{\max} \tag{3.48}$$

In this model the damage variable was set equal to the ratio of the current strain and the maximum strain in the loading history.

De Souza Neto *et al.* (1994) introduced a similar model in which the softened stress is related to the engineering stress, $\mathbf{P}_o$, in the *virgin* material, i.e.,

$$\mathbf{P} = F(\xi)\mathbf{P}_o \tag{3.49}$$

Here, $\mathbf{P}_o$ is determined from the hyperelastic theory introduced previously such that

$$\mathbf{P}_o = \frac{\partial \psi_o(\mathbf{F})}{\partial(\mathbf{F})} \tag{3.50}$$

In the De Souza Neto *et al.* (1994) model, the damage variable is defined with reference to the maximum value of the strain energy density, D, i.e.,

$$\xi = \frac{\psi_o}{D} \tag{3.51}$$

Beatty and Zúñiga (2002) adopt a phenomenological model for the stress softening that is quite easy to implement. In their model, the Cauchy stress in the *damaged* material, **T**, is related to the Cauchy stress in the *undamaged* material, $\mathbf{T_o}$, through a scalar-valued damage function, F(m;M), i.e.,

$$\mathbf{T} = F(m;M)\mathbf{T}^o \tag{3.52}$$

As in the previous models, the damage is dependent upon the previous maximum deformation, resulting in a *memory* effect. Beatty *et al.* (2002) implement the strain intensity *m* to track the magnitude of the deformation and then determine the degree of softening, i.e.,

$$m = \sqrt{\mathbf{bb}} = \sqrt{tr(\mathbf{b}^2)} = \sqrt{(\lambda_1^4 + \lambda_2^4 + \lambda_3^4)} \quad , \tag{3.53}$$

where **b** is the left Cauchy-Green deformation tensor and λ_i are the principal stretches. The maximum deformation, m_{max}, is then denoted by M. The *ideal* Mullins behavior requires that **T** vanish when the material is returned to the stress-free state. This condition is satisfied through the definition of $\mathbf{T}^o$, which is zero when the material is not deformed which corresponds to $\lambda_1 = \lambda_2 = \lambda_3 = 1$ or $m = \sqrt{3}$.

Additionally, since the Mullins effect is a *softening* phenomenon, the damage function cannot *exceed* unity and must be *identically* unity at M; such that the stress at M is the same in *both* the *damaged* and *undamaged* material. From 3.43 and the constraints just described, $F(m;M)$ is subject to the following constraints

$$0 \le F(m;M) \le 1$$
$$F(M;M) = 1 \tag{3.54}$$

Based on these constraints, Beatty *et al* adopted the following form for the damage function, $F(m;M)$:

$$F(m;M) = e^{-b\sqrt{(M-m)}} \tag{3.55}$$

The *softening parameter*, b, determines the degree of softening that the material undergoes and can be fit from experiments to specific materials. Substitution of $F(m;M)$ into the relation for **T**, the stress in the *damaged* material becomes

$$\mathbf{T} = e^{-b\sqrt{M-m}}\mathbf{T}^o \tag{3.56}$$

In an *idealized* Mullins material, the stress behavior during reloading for strain intensities greater than the previously *memorized* value maximum M will revert back to the response of the virgin material. Therefore, the stress is evaluated in a manner dependent upon current state of m, i.e.,

$$\begin{aligned}
&\mathbf{T} = \mathbf{T}^o && \text{for } \textit{initial} \text{ loading in which } m=M \\
&\mathbf{T} = e^{-b\sqrt{M-m}}\mathbf{T}^o && \text{for unloading and reloading } 0<m<M \\
&\mathbf{T} = \mathbf{T}^o && \text{for reloading where } m>M
\end{aligned} \tag{3.57}$$

This theory is simpler than those mentioned above and was shown to match experimental data quite well. Unfortunately, none of these models capture any irreversibility or difference between loading and unloading paths observed for goose down.

CHAPTER IV

PROPOSED MODEL

The fiber network models discussed in the previous chapter focus on determining the amount of elastic energy stored within a mass of fibers, based primarily on the elastic bending energy stored in each individual fiber. These models idealize the network of fibers in an attempt to capture all of the micromechanics that contribute to the overall behavior. Unfortunately, the relationships developed within those models become very complex and rely on parameters that are difficult to determine experimentally. Furthermore, it can be argued that the network of wool and synthetic fibers studied in those models differs greatly from the hierarchical morphology of goose down. Some of the concepts from these models are still applicable; fiber bending is still the primary mechanism for storing elastic energy and occurs as a result of fiber contact, and orientation plays an important role as well. The phenomenological models used to describe the behaviors of certain rubbers are appealing due to their mathematical simplicity, but are less desirable because they lack any reference to the internal mechanisms of the material. The molecular network theory incorporates chain physics making them more accurate and can serve as a loose guide for the development of the proposed model for goose down.

The proposed model seeks to define a unique strain-energy function that has physical significance related to the internal mechanisms of goose down that were discussed in Chapter II. Once the strain-energy function has been developed, the

principal stresses in the material will then be determined from the hyperelastic theory and an approach similar that of Beatty and Zúñiga to model the ideal Mullins effect.

4.1 The Proposed Model

The purpose of this model is to capture the physical response of goose down by considering a spherical representative volume element (RVE) that is fixed in space and subjected to cyclic compressive strains. The RVE is sufficiently large that thousands of goose down clusters are present. In order to further simplify the model, several assumptions are made:

1. The material is initially random and can be considered to be isotropic.
2. The material is homogenous.
3. The principal stretch axes are coaxial with the principal material directions.
4. All elastic energy storage occurs through deformation of the secondary structures due to tertiary-to-tertiary contacts.
5. Tertiary structures are responsible for pinning some of the secondary structure.
6. The Poisson's ratio is assumed to be zero.

The material is assumed to be initially isotropic so that the principal material and deformation directions can be chosen to coincide. Therefore, the model can be best posed in terms of the principal stretches, λ_i, in a manner that satisfies the frame indifference requirement.

It is assumed that secondary structure bending is the primary source for stored elastic energy within the system. Assuming that significant elastic energy only develops in a secondary structure when two tertiary structures engage, the energy developed within

the RVE depends directly on the number of tertiary contacts that are created. Quantifying the tertiary-to-tertiary contacts then becomes the focus in developing the strain-energy function. The number of tertiary engagements is assumed to depend upon the primary structure orientation and average tertiary density within the RVE. Once the strain energy function has been determined, the stress can be calculated using the hyperelasticity theory and a slight modification of the Beatty *et al*. (2002) model for an idealized Mullins material.

4.2 Orientation Effects

It is assumed that more tertiary contacts will form as a greater proportion of secondary structures become oriented *toward* the loading direction. From Chapter II, the secondary structures branch from the primary structures at approximately 90°, implying that more secondary structures are oriented *in* the loading direction as more primary structures align *away* from the direction of compressive deformation. Therefore, it is necessary to incorporate a statistical quantity related to the primary structure orientation.

The micromechanical fiber network models for wool (Komori *et al* 1999, Carnaby *et al.* 1989) incorporate orientation distribution functions (ODF) in order to account for orientation effects. In practice, an ODF is difficult to determine for a complex three-dimensional material like goose down. In place of a rigorously defined ODF, a *fabric ellipsoid* will be implemented to convey the essence of the primary structure arrangement without invoking a higher degree of freedom (DOF) model. The fabric ellipsoid and its related fabric tensor have been used in the study of porous and granular materials by Cowin (1985, 1987) and Oda *et al.* (1980), respectively.

The fabric tensor is a second-rank and positive-definite tensor that physically represents a *fabric ellipsoid*. The fabric ellipsoid provides an overall description of any preferential alignment of the primary structures occurring within the RVE. The principal values of the fabric tensor are inversely related to the magnitudes of the major and minor axes of the fabric ellipsoid. If the fabric tensor associated with the primary structures, $\mathbf{\Omega_P}$, has principal values equal to ϖ_i, then the axes of the associated primary structure orientation ellipsoid (PSOE), ω_i, are given by,

$$\omega_i = \frac{2}{\sqrt{\varpi_i}} \tag{4.1}$$

The magnitudes of these axes are related to the ODF associated with the primary structures. The lengths of the ellipsoidal axes are analogous to the relative proportion of primary structures oriented in the direction associated with that axis. For example, a sample of goose down with an initially random (isotropic) primary structure orientation distribution will be have a PSOE in the shape of a sphere. After uniaxial compression, the primary structures will reorient and the PSOE will be an oblate spheroid as shown in Figure 4.2.1. The ellipsoidal axes in the first and second principal directions increase by an equal amount and will now be greater than the axis in the third principal direction. The shorter axes in the third principal direction relates to statistically *fewer* primary structures oriented in that direction. Based on the assumption relating secondary and primary orientations, more secondary structures would then be oriented in the direction of compression.

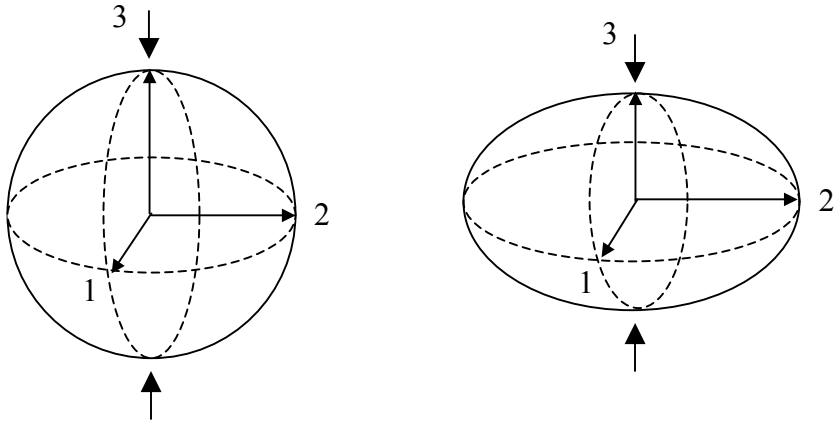

(a) (b)

Figure 4.2.1 (a) Initial PSOE for a RVE with random orientation distribution of primary structures (isotropic). (b) The PSOE for the deformed RVE after compression in the 3rd principal direction resulting in a preferential alignment of primary structures in 1st and 2nd principal directions

The stretch tensor, **U**, is also symmetric and positive-definite, and itself represents an ellipsoid. Therefore, $\mathbf{\Omega_P}$ could be expressed directly as a tensor function of the stretch tensor as long as the result is still symmetric and positive-definite. For this model, the principal axes of $\mathbf{\Omega_P}$ and the principal stretch directions remain aligned, and the axes of the primary structure orientation ellipsoid can be derived directly in terms of the principal stretches, i.e.

$$\omega_1 = \omega_{10} - \langle 1-\lambda_1 \rangle^{\gamma} \omega_{10} + \frac{1}{2}\langle 1-\lambda_2 \rangle^{\gamma} \omega_{20} + \frac{1}{2}\langle 1-\lambda_3 \rangle^{\gamma} \omega_{30}$$

$$\omega_2 = \omega_{20} + \frac{1}{2}\langle 1-\lambda_1 \rangle^{\gamma} \omega_{10} - \langle 1-\lambda_2 \rangle^{\gamma} \omega_{20} + \frac{1}{2}\langle 1-\lambda_3 \rangle^{\gamma} \omega_{30}$$

$$\omega_3 = \omega_{30} + \frac{1}{2}\langle 1-\lambda_1 \rangle^{\gamma} \omega_{10} + \frac{1}{2}\langle 1-\lambda_2 \rangle^{\gamma} \omega_{20} - \langle 1-\lambda_3 \rangle^{\gamma} \omega_{30} \qquad (4.2)$$

Any initial alignment due to a prior compaction of the material is accounted for through the initial values of the PSOE axes, ω_{i0} (i =1,3). The above equations satisfy the requirement that $\omega_{i0}=\omega_i$ for the undeformed state in which $\lambda_i = 1$ (i = 1,3). In uniaxial compression, fibers rotate away from the direction of compression resulting in a *shorter* axis. In accordance with a sphere representing an initially random (isotropic) primary structure orientation distribution, $\omega_{io} = 1$. Macaulay brackets, < >, are used here to denote:

$$\begin{aligned} \langle 1-\lambda_i \rangle^{\gamma} &= (1-\lambda_i)^{\gamma} \quad \text{if } (1-\lambda_i) \geq 0 \\ \langle 1-\lambda_i \rangle^{\gamma} &= 0 \qquad\quad \text{if } (1-\lambda_i) < 0 \end{aligned} \tag{4.3}$$

The use of Macaulay brackets here suggests that only compressive deformation will influence the orientation. The exponent, $\gamma \geq 1$, is used here to add generality to the model. In this work, γ will considered to be a constant throughout the deformation although in reality it may depend on the initial density of the material and may evolve with deformation. The effect of γ in the case of uniaxial compression will be discussed in Chapter V.

It should be noted that the fabric ellipsoid and spherical RVE do not necessarily deform identically. In fact, the deformation of the PSOE is probably somewhat retarded compared to the deformation of the RVE due to density effects. Also, if the fabric ellipsoid is used as a true ODF, then the axes should be normalized so that their sum is unity. As the axes are defined above, their sum will always be equal to $\omega_{10}+\omega_{20}+\omega_{30}$, allowing them to be easily normalized.

As mentioned above, it has been postulated that the number of tertiary-to-tertiary engagements increases as more primary structures become oriented *away* from the direction of a compressive load. Therefore, it is desirable to have a parameter that conveniently relates the degree of primary *alignment* orthogonal to the loading direction. A ratio of the PSOE axes normal to the loading direction, to the PSOE axis in the loading direction conveniently represents the degree of primary structure *alignment away* from the loading direction. These ratios, η_i, can then be expressed as a function of the PSOE axes, i.e.

$$\eta_1 = \frac{\omega_2 + \omega_3}{2\omega_1} \quad \eta_2 = \frac{\omega_1 + \omega_3}{2\omega_2} \quad \eta_3 = \frac{\omega_1 + \omega_2}{2\omega_3} \tag{4.4}$$

Defined in this manner, η_i will *increase* for compression in the i^{th} direction, indicating that *fewer* primary structures (*more* secondary structures) are oriented in the i^{th} direction. For an initially random material, all of the η_i are equal to unity. Using these ratios also eliminates the need to normalize the axes. These orientation ratios represent the *alignment* of the primary structures relative to a specific direction, which is more meaningful than the axes of the PSOE alone. These ratios will be directly implemented into the expression for the number of tertiary-to-tertiary contacts.

4.3 The Number of Tertiary-to-Tertiary Engagements

It is assumed that number of tertiary contacts occurring within the RVE depends on the average tertiary structure density and orientation of the primary structures. The

density influence can be accounted for through the third invariant I_3, sometimes denoted by J, which is related to the change in volume, i.e.

$$I_3 = \det \mathbf{F} = \lambda_1 \lambda_2 \lambda_3 = \frac{dV}{dV_0} = \frac{\rho_0}{\rho} \tag{4.5}$$

The density will be incorporated into the equation for the number of tertiary contacts through the inclusion of the reciprocal of the third invariant, $1/I_3$.

It is postulated that contacts will have a tendency to accumulate more rapidly as the primary structures become more aligned in the plane orthogonal to the loading direction. The ratios defined above have been defined such that they increase as the primary alignment out of loading direction also increases. Only compression will be considered here and the Macaulay brackets will be implemented once more. The equation for the number of tertiary contacts per unit reference volume, N_{TT}, can be expressed as a function of the principal stretches, λ_i, the third invariant, I_3, and the orientation ratios, η_i, i.e.

$$N_{TT} = \frac{1}{V_0}\left[\frac{\beta}{I_3^N}\left(\langle 1-\lambda_1\rangle^{\alpha_1}\eta_1^{\alpha_2} + \langle 1-\lambda_2\rangle^{\alpha_1}\eta_2^{\alpha_2} + \langle 1-\lambda_3\rangle^{\alpha_1}\eta_3^{\alpha_2}\right)\right] \tag{4.6}$$

Here β is a constant that will be dependent upon the total number of tertiary structures contained within the RVE. The exponent, N, influences the effect that density has on number of tertiary contacts. The latter terms in the expression for N_{TT} incorporate the orientation influence on the total number of tertiary contacts through the incorporation of the orientation ratios, η_i. The above equation implies a coupling

between the deformation direction and contact formation through the inclusion of the orientation ratios.

4.4 The Behavior of a Contact

Another complicating factor of the micromechanics approaches is determining the magnitude of the force at a single contact. Most of the previous models for wool fiber assemblies have assumed a constant contact force (Carnaby et al. 1989); however, the finite element model of Beil *et al*. (2002A/B) suggests that the contact force is neither constant nor equal among contacts. One possible way of simplifying this problem is to assume that the energy stored per contact follows a statistical distribution. The distribution will be allowed to evolve with deformation to reflect the change in elastic energy storage within the contacts. Such an assumption can be justified by observing that during initial compression there are fewer contacts, but they are associated with larger elastic secondary deformations. As the primary structure orientation changes, the contacts become more stable and the average secondary deformation is not as large, resulting in a greater number of contacts which, on average, store less energy. The total stored elastic energy of the RVE continues to increase despite the lower average contact energy since N_{TT} continues to increase nonlinearly.

The energy associated with each contact is assumed to lie between zero and a maximum energy, E_{ctmax}, associated with a large secondary structure deformation. The fraction of N_{TT} that are associated with a specific contact energy, E_{ct}, is determined from the distribution function $g(E_{ct})$. A function is needed that can be evolved with the change

in primary structure orientation. A possible general form of the distribution function for the normalized contact energies, $g(E_{ct})$ is given by

$$g(E_{ct}) = B\frac{f(\max\eta_i)A^{f(\max\eta_i)E_{ct}\frac{c}{E_{ct\max}}}}{A^{f(\max\eta_i)c}-1} \tag{4.7}$$

The constant, c, has some influence on the shape of the distribution. The constant B needs to be determined such that $g(E_{ct})$ satisfies the normalization condition (Hayter, 2002) for any probability distribution function, i.e.,

$$\int_0^{E_{ct\max}} g(E_{ct})dE_{ct} = 1 \tag{4.8}$$

Applying the normalization condition, and noting that $f(\max\ \eta_i)$ and $E_{ct\max}$ are constant for a given increment, leads to the following expression

$$B = \ln A \tag{4.9}$$

Substitution of B back into the general form for $g(E_{ct})$ renders

$$g(E_{ct}) = \ln A\frac{f(\max\eta_i)}{A^{f(\max\eta_i)c}-1}A^{f(\max\eta_i)E_{ct}\frac{c}{E_{ct\max}}} \tag{4.10}$$

The distribution function depends on the degree of primary alignment through the function $f(\max\ \eta_i)$, i.e.,

$$f(\max \eta_i) = C - \left|\max \eta_i - \eta_{i0}\right| \tag{4.11}$$

The quantity $\left|\max \eta_i - \eta_{i0}\right|$ relates to the total change in *alignment* of the primary structures that has occurred. The constant C determines how much the distribution will evolve. If $\left|\max \eta_i - \eta_{i0}\right| = C$, the energy per contact will be uniformly distributed between 0 and $E_{ct\max}$.

Another benefit of using a distribution to describe the energy per contact is that it is only necessary to calculate the energy associated the assumed maximum elastic deformation of a single secondary structure, E_{ctmax}. In order to simplify the determination of the bending energy, an idealized deformation of a secondary structure into a circle is used as shown in Figure 4.4.1

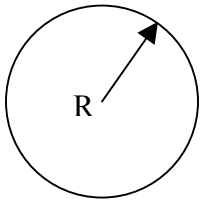

Figure 4.4.1 Representative *maximum* deformation of a single secondary structure due to contact between secondary structures.

If the length of an initially straight secondary structure is l_f, then the radius, R, of the deformed secondary is equal to $l_f/2\pi$. The solution to a linear elastic flexible bar bent

into a complete circle was solved using the elastica solution by Frish-Fay (1962). He determined the strain energy stored in an initially straight bar of length $4l_f$ to be:

$$U = \frac{B_f \pi^2}{2l_f} \tag{4.12}$$

For a single secondary of length l_f, E_{ctmax} is then given according to

$$E_{ct\max} = \frac{2B_f \pi^2}{l_f} \tag{4.13}$$

The flexural rigidity, B_f, is given according to $E_f I_f$, where E_f is the Young's Modulus and I_f is the moment of inertia and is equal to $(1/4)\pi r_f^4$ for a round cross-section.

The strain-energy density of the RVE, Ψ, for a given deformation state can be given by the summation of the elastic energy stored in each of the secondaries associated with the tertiary contacts, i.e.,

$$\Psi = N_{TT} \int_0^{E_{ct\max}} E_{ct} g(E_{ct}) dE_{ct} \tag{4.14}$$

In this expression, N_{TT}, is the total number of contacts per unit reference volume and the integral determined the expected energy per contact based on the distribution function $g(E_{ct})$.

4.5 Determining Stress

For a strain energy function describing a hyperelastic, isotropic material derived in terms of the principal stretches, the principal nominal stresses, P_i, can be found by differentiating the strain energy, Ψ, with respect to the respective principal stretch, λ_i (Holzapfel 2000) i.e.,

$$P_i = \frac{\partial \Psi}{\partial \lambda_i} \tag{4.15}$$

Likewise, the principal Cauchy stress is given by

$$\sigma_i = I_3^{-1} \lambda_i \frac{\partial \Psi}{\partial \lambda_i} \tag{4.16}$$

These relations are only valid for the initial loading of the material since they are defined for a material that behaves elastically with coincident loading and unloading paths. An approach similar to the one developed by Beatty *et al.* (2002) to model the stress softening behavior of an idealized Mullins material will be implemented to determine the stress during the recovery and reloading stages. The experimental behavior of goose down varies from that of an *idealized* Mullins material and requires a slight modification of the Beatty *et al.* model. In particular, goose down exhibits irreversible deformation as well as different loading and unloading paths, whereas an ideal Mullins material is perfectly elastic and has coincident reloading and unloading paths.

In the Beatty *et al.* (2002) model, the stress during reloading and unloading is related to the stress response for the *virgin* material. The response in these subsequent paths depends on the deformation history, namely there is a *memory effect* of the maximum deformation. Beatty *et al.* tracked the deformation history using the strain intensity, m, which can be defined in terms of the principal stretches i.e.,

$$m = \sqrt{(\lambda_1^4 + \lambda_2^4 + \lambda_3^4)} \tag{4.17}$$

The maximum deformation is associated with the maximum strain intensity, M, and can be expressed in terms of the *minimum* principal stretches, $\lambda_i^{\min}$, corresponding to the maximum compression, i.e.,

$$M = \sqrt{(\lambda_1^{\min})^4 + (\lambda_2^{\min})^4 + (\lambda_3^{\min})^4} \tag{4.18}$$

The deformation associated with M can also be thought of as the deformation from which unloading occurs.

The stress in the subsequent cycles can then be determined from the stress in the *virgin* material, $\mathbf{T}^o$, and a softening function $F(m;M)$, i.e.,

$$\mathbf{T} = \mathbf{T}_o \quad \text{loading of virgin material and loading reloading when } m>M$$

$$\mathbf{T} = \mathbf{T}_o e^{-b\sqrt{(M-m)}} \quad \text{reloading and unloading for } m<M \tag{4.19}$$

where $F(m;M)$ is defined by

$$F(m,M) = e^{-b\sqrt{m-M}} \tag{4.20}$$

As outlined above, the Beatty *et al.* (2002) model is not able to model materials that exhibit irreversible behavior. It is assumed that the irreversible deformation observed in goose down is due to secondary deformations and the permanent reorientation of the primary structures. The irreversible deformation leads to a new stress-free state and a *new* reference configuration. Stretches in this *new* configuration will be denoted by λ_i^*, while stretches in the reference configuration will use the existing notation.

The new stress-free state is dependent upon the proportion of deformation that is reversible. The minimum stretch, λ_i^{min}, can be partitioned into a reversible portion, λ_i^R, and irreversible component, λ_i^{IR}. It is proposed that λ_i^R depends on the minimum stretches, λ_i^{min}, and alignment of the primary structures. Therefore, λ_i^R can be expressed a function of the minimum stretch in that direction and the associated orientation ratio η_i,,

$$\lambda_i^R = R(\eta_i, \lambda_i^{max}) \tag{4.21}$$

where

$$R(\eta_i, \lambda_i^{max}) = \hat{R}(\eta_i)(1-\lambda_i^{max}) \qquad 0 < \hat{R}(\eta_i) < 1 \tag{4.22}$$

$\hat{R}(\eta_i)$ is a function of the orientation ratio, η_i, and determines the proportion of the stretch that is reversible. It is assumed that as the primary structures become more aligned, $\hat{R}(\eta_i)$ will increase as the orientation ratio, η_i, differs from its initial value η_{io}. In the case of an initially random material, η_{io} will equal unity.

For compression, the stretch in the *original* configuration corresponding to the new stress-free state is determined from

$$\lambda_i^{IR} = \lambda_i^{\max} + \lambda_i^{R} \tag{4.23}$$

The new stress-free state and the corresponding stretches in the *original* and *new* configurations are shown in Figure 4.2.3.

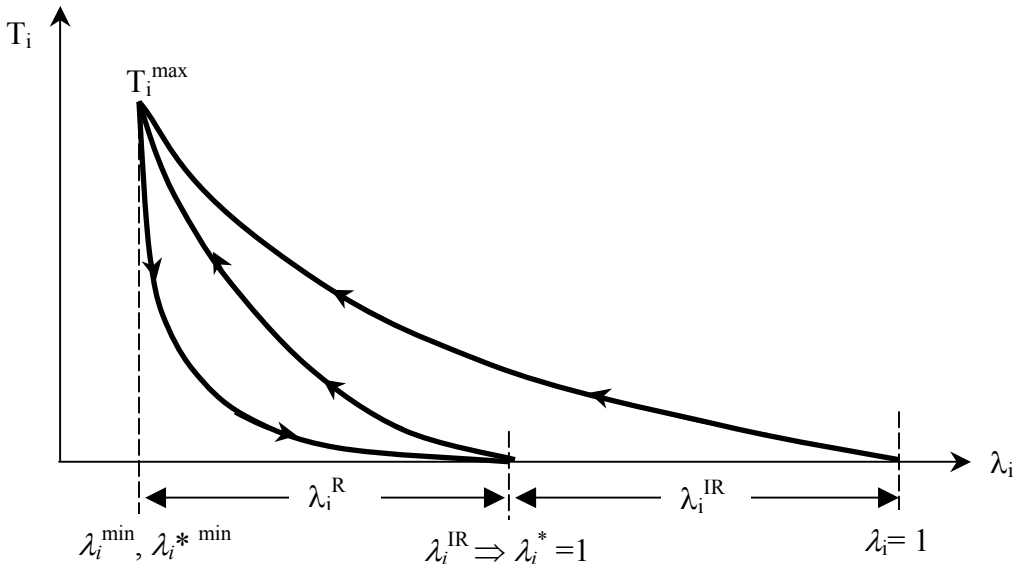

Figure 4.5.1 Representation for irreversible behavior with different reloading and unloading paths.

Likewise, the stretch in the *new* configuration corresponding to λ_i^{IR} is $\lambda_i^* = 1$ as shown in Figure 4.2.3.

The strain intensity in the new configuration also becomes,

$$m^* = \sqrt{(\lambda_1^*)^4 + (\lambda_2^*)^4 + (\lambda_3^*)^4} \tag{4.24}$$

and the maximum strain intensity in the new configuration, M^* is defined

$$M^* = \sqrt{(\lambda_1^{*\min})^4 + (\lambda_2^{*\min})^4 + (\lambda_3^{*\min})^4} \tag{4.25}$$

The new stress free state occurs when $m^* = \sqrt{3}$, corresponding to $\lambda_i^* = 1$. Similarly, the maximum stress state in the initial loading, $\mathbf{T}^o$, occurred at $m = M$ and now that same stress state must occur when $m^* = M^*$.

As discussed above, the Beatty *et al.* (2002) model relates the stress in the unloading and reloading paths to the stress developed during the initial loading of the *virgin* material, $\mathbf{T}^o$. For an elastic material, there is no change in the stress free state and the *virgin* material response can be used directly. For an irreversible deformation, the shifting of the stress-free state and change in reference configuration require the definition of a new scaled stress, $\hat{\mathbf{T}}^o$, to be used in the place of $\mathbf{T}^o$.

For a given deformation defined in the *new* configuration, $\hat{\mathbf{T}}^o$ has a value corresponding to a specific stress in the compression of the virgin material, $\mathbf{T}^o$. Specifically, the stress in the *current* stress-free state *must* correspond to the stress in the *original* stress free state. Likewise, the maximum deformation in the *new* and original

configurations *must* result in the same peak stress. Accordingly, $\hat{\mathbf{T}}^{o}$, must satisfy the following constraints.

$$\hat{\mathbf{T}}_{o}(\lambda_i^{*}=1)=0=\mathbf{T}^{o}(\lambda_i=1)$$

$$\hat{\mathbf{T}}^{o}(\lambda_i^{*}=\lambda_i^{*\min})=\mathbf{T}^{o\max}=\mathbf{T}^{o}(\lambda_i=\lambda_i^{\min}) \tag{4.26}$$

The constraints above suggest that if a relationship between m and m^{*} can be found, then $\hat{\mathbf{T}}^{o}$ can be evaluated in terms of the stress developed in the *virgin* material, $\mathbf{T}^{o}$. Since m can be expressed in terms of the principal stretches, a relationship between the stretches in the *new* and *original* configuration can be used to determine the corresponding strain intensity in the *original* configuration, m, based on the strain intensity in the *new* configuration, m^{*}. Given a stretch in the *new* configuration, a corresponding scaled stretch, λ_i' in the *original* configuration can be defined according to

$$\lambda_i'=1-\left(\frac{1-\lambda_i^{*}}{1-\lambda_i^{*\min}}\right)(1-\lambda_i^{\min}) \tag{4.27}$$

For $\lambda_i^{*}=1$, the expression yields $\lambda_i'=1$ which correctly implies that a stretch in the new configuration should map to $\lambda_i=1$ in the original configuration. Likewise, for $\lambda_i^{*}=\lambda_i^{*min}$ the scaled stretch is $\lambda_i'=\lambda_i^{\min}$. From this relationship, the scaled stress can be equated to the proper stress in the virgin material,

$$\hat{\mathbf{T}}^o(\lambda_1^*, \lambda_2^*, \lambda_3^*) = \mathbf{T}^o(\lambda_1', \lambda_2', \lambda_3') \tag{4.28}$$

An ideal Mullins material reloads and unloads along the same curves for deformations satisfying m<M. Due to the configuration of the tertiary structures, the unloading behavior of goose down is significantly different from the loading of the virgin material and reloading of the reoriented material.

The Beatty *et al.* (2002) has been derived for an ideal Mullins material and uses two relations to describe the stress; one relation for loading and the other for unloading and reloading where $m<M$. In order to include the distinct unloading path exhibited by goose down, a third stress relation will be added. This additional unloading relationship will be distinguished from the reloading relationship due to a different *softening parameter*, b_U. The reloading and unloading stress relations have different *softening parameters*, denoted by b_R and b_U, respectively such that the three expressions for the stress developed within a sample of goose down are,

$$T_i^o = \frac{\partial \Psi}{\partial \lambda_i} \quad \text{for loading of the } \textit{virgin} \text{ material, m=M, } \dot{m} < 0$$

$$T_i = \hat{T}_i^0 e^{-b_u\left(m^* - M^*\right)^a} \quad \text{for unloading, } \dot{m} < 0 \text{ from m=M.}$$

$$T_i = \hat{T}_i^0 e^{-b_R\left(m^* - M^*\right)^a} \quad \text{for reloading, } \dot{m} < 0 \text{ and m<M} \tag{4.29}$$

In the equations above, the softening function has been generalized by the addition of the exponent a, which was equal to ½ in the Beatty *et al.* (2002)model. The generalization is justified since goose down is an entirely different material than the

rubber materials modeled by Beatty *et al.* (2002). Another possible form for the softening function is,

$$F(m;M) = e^{-b\left((m^*)^a-(M^*)^a\right)} \tag{4.30}$$

This alternative form still satisfies the constraint that $F(m;M)$ equals unity when $m = M$ and the constants b and a may have different values for loading and unloading.

The values of b_R and b_U may also be functions of the orientation state at the point from which unloading begins. It might be expected that b_U would decrease as the material becomes more aligned and compacted. This would decrease the amount of hysteresis and seems intuitive. A possible expression for the value of b_U could be,

$$b_U = \left(\frac{1}{\max \eta_i}\right)^{\alpha_U} C_U \tag{4.31}$$

where the maximum orientation ratio, max η_i, will increase from unity as the material become more aligned causing b_U to decrease as alignment increases, and α_U is constant.

In a typical Mullins material the response for the *virgin* material is invoked for $m>M$. As of yet, there is no experimental evidence available to suggest whether goose down reverts back to the initial loading curve or maintains a path closer to that of the reloading curve once the loading exceeds the previous maximum strain intensity. Once the proper behavior has been determined experimentally it can be incorporated into the

model through the addition of a simple conditional statement that tells the model which stress relation should be used.

The model outlined above captures the essence of the behavior of goose down in compression while incorporating some of the microstructural details through the use of a unique strain energy density function. The general algorithm for the model is presented in Figure 4.5.2. As this model is only a first attempt to capture the behavior of goose down there is much work that can be pursued further to enhance the model to make it more accurate and robust. Detailed suggestions, as well as results for uniaxial compression, will be presented in the next chapter.

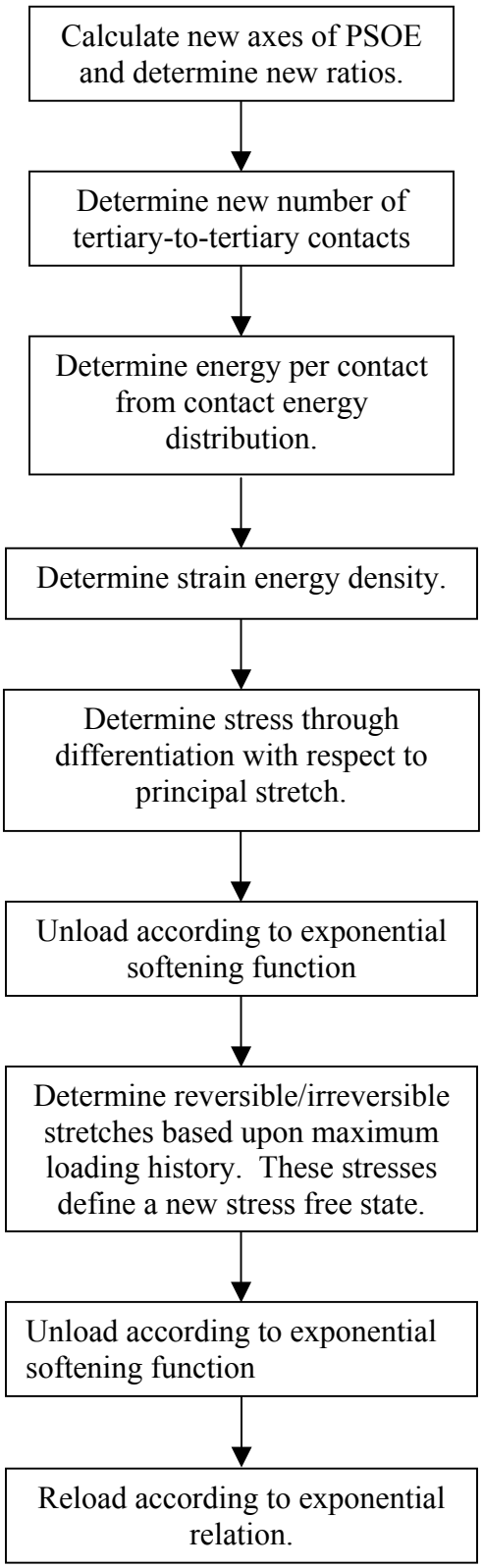

Figure 4.5.2 Flow diagram of proposed model.

CHAPTER V

EVALUATION OF THE PROPOSED MODEL

The proposed model was evaluated for uniaxial compression. Assuming that goose down has a Poisson's ratio of zero, the principal stretches for uniaxial compression simplify to $\lambda_1 = \lambda$ and $\lambda_2 = \lambda_3 = 1$. The equations for the axes of the PSOE then become,

$$\omega_1 = \omega_{10} - \langle 1-\lambda \rangle^{\gamma} \omega_{10}$$

$$\omega_2 = \omega_{20} + \frac{1}{2}\langle 1-\lambda \rangle^{\gamma} \omega_{10}$$

$$\omega_3 = \omega_{30} + \frac{1}{2}\langle 1-\lambda \rangle^{\gamma} \omega_{10} \qquad (5.1)$$

Furthermore, if the primary structures have an initial random orientation distribution, then $\omega_{10} = \omega_{20} = \omega_{30} = 1$ which leads to $\omega_2 = \omega_3$ and $\eta_2 = \eta_3$.

For uniaxial compression, the primary structure orientation distribution in the direction of compression is the most important. For this simplified case, it is easy to explore the influence that γ has on the evolution of the PSOE axes. In particular, ω_1 has been plotted against λ for γ=1, 1.5, 2, and 2.5 as shown in Figure 5.1.1.

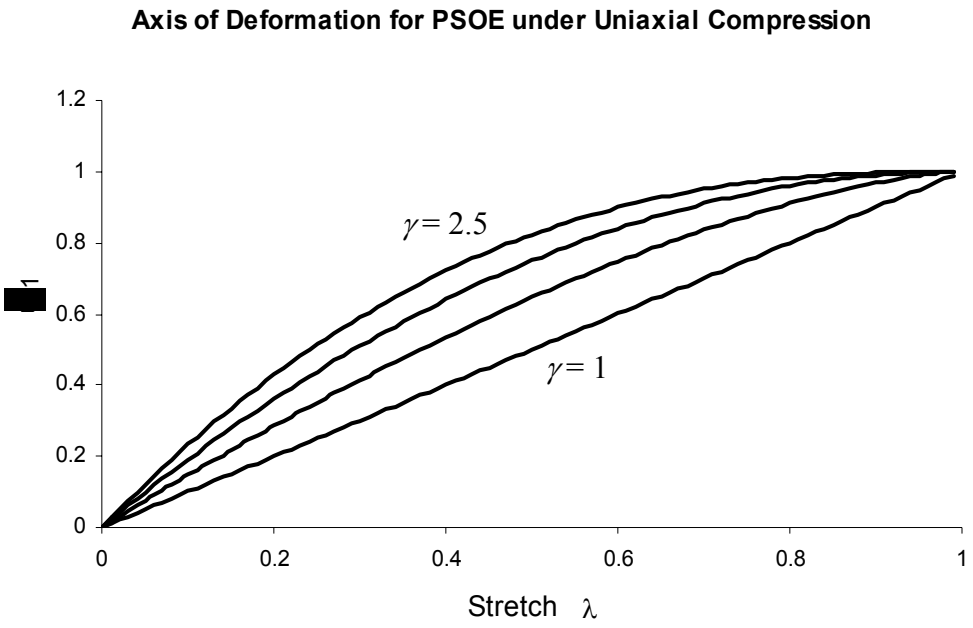

Figure 5.1.1 Influence of the exponent, γ, on the PSOE axis in uniaxial compression for γ=1.0, 1.5, 2.0, 2.5

From Figure 5.1.1, it is easy to see that increasing γ delays the change in orientation of the primary structures relative to the stretch. When $\gamma = 1$, ω_1 is equal to λ and the PSOE deforms in unison with the RVE. In reality, there is probably a delay, and the value of γ is likely to be highly dependent on the initial density of goose down contained in the RVE. This variable may also evolve with deformation, however, for evaluations of this model in the present work it will be held constant.

For uniaxial compression, the influence of the primary structure orientation is based on the proportion of primary structures oriented *away* from the loading direction. For uniaxial compression in the first principal direction, the degree of primary structure alignment is given through the orientation ratio η_1, and is plotted against stretch (for γ = 2.0) in Figure 5.1.2.

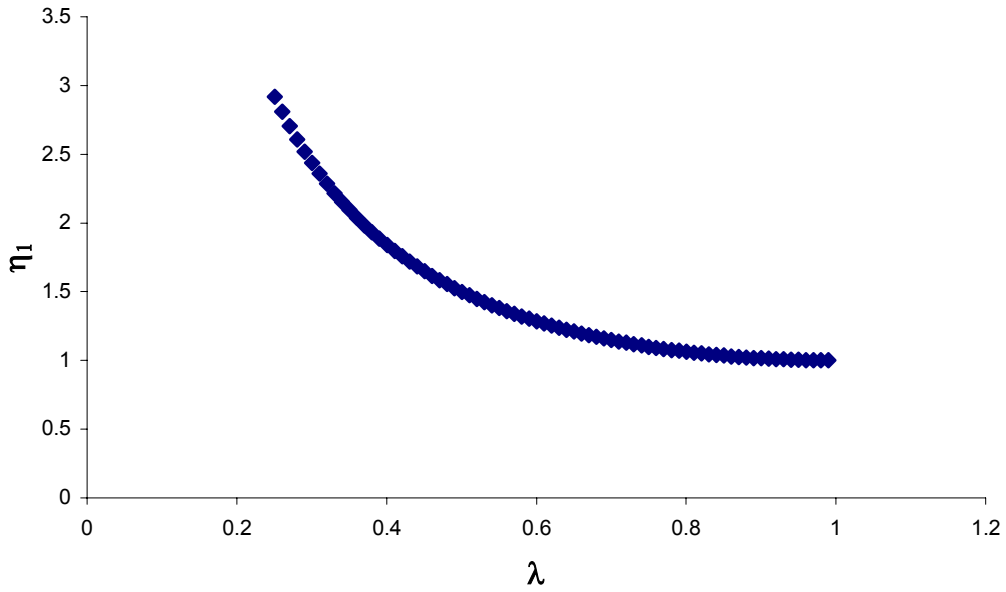

Figure 5.1.2. Primary structure orientation ratio, η_1, plotted vs. applied stretch.

For an initially random material, the value of η_1 increases nonlinearly from one. This suggests that the proportion of primary structures oriented *away* from the first principal direction increases nonlinearly with stretch and is expected due to the nonlinear behavior of ω_1 shown in Figure 5.1.1.

The equation for the number of tertiary contacts per unit reference volume also simplifies in uniaxial compression where the third invariant, I_3, simplifies to λ, and N_{TT} is given by

$$N_{TT} = \frac{1}{V_0}\left[\frac{\beta}{\lambda^N}\langle 1-\lambda\rangle^{\alpha_1}\eta_1^{\alpha_2}\right] \tag{5.2}$$

The exponent, N, affects how much of an effect the change in density has on N_{TT} as shown in Figure 5.1.3 for $\beta = 500$. It should be noted that for a dilatational loading, λ_1 =

$\lambda_2 = \lambda_3 = \lambda$, the density will change with λ^{3N}. The other exponents, α_1 and α_2, are included to add more flexibility in fitting the model to further experimental results. As mentioned above, the value of β is related to the quantity of goose down contained in the RVE and the total number of tertiary structures.

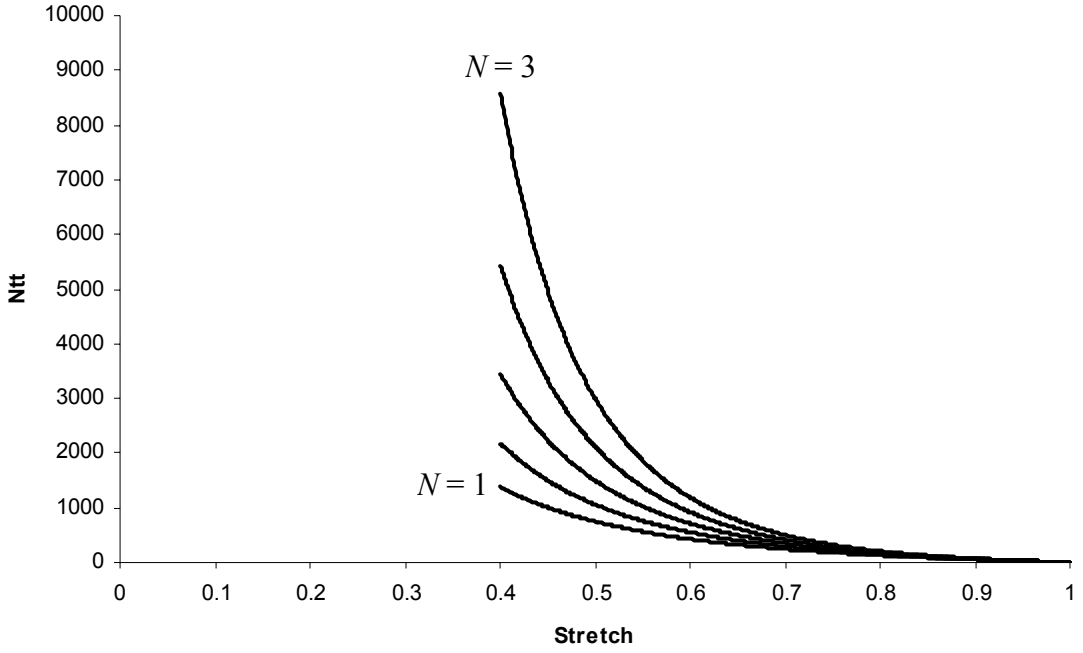

Figure 5.1.3 Total number of tertiary-to-tertiary contacts vs. stretch for $\beta = 500$ and $N = 1, 1.5, 2, 2.5, 3$

The maximum energy present in a single secondary was calculated using the Young's modulus, 1.31GPa, determined by Bonser (1999) for a single primary structure. The secondary structure diameter was estimated to be 0.005 mm. Assuming an average secondary length of 0.65mm, the value of E_{ctmax} was estimated to be 0.1236 nJ. The contact energy distribution was evaluated for $A = 1.4$ and $C = 0.2$, and $c = 10$. Using this distribution, the average energy per contact will decrease as alignment of the primary

structures increases. If $\gamma = 3$, the average energy per contact will decrease from an initial energy of 0.07 nJ for $\lambda = 1$ to 0.057 nJ when $\lambda = 0.44$.

For uniaxial compression, the strain intensity, *m*, and maximum strain intensity, *M*, used in the stress relations also simplify,

$$m = \sqrt{\lambda_1^4 + 2} \qquad M = \sqrt{(\lambda_1^{\min})^4 + 2} \tag{5.3}$$

In the current evaluation of the model, the irreversible stretch was determined by

$$\lambda^R = \frac{1}{2}(1 - \lambda^{\min}) \tag{5.4}$$

where the factor ½ was approximated from the experimental data.

The stress-displacement response was evaluated for an element with a diameter of .25m subjected to successive stretches of decreasing magnitudes (increasing compression) from $\lambda^{\min} = 0.66$ to $\lambda^{\min} = 0.44$. In evaluating the stress, one of the more general forms of the damage functions discussed in Chapter IV was implemented such that the stress relations take the forms,

$$T_i^o = \frac{\partial \Psi}{\partial \lambda_i} \quad \text{for loading of the } \textit{virgin} \text{ material, m=M, } \dot{m} < 0$$

$$T_i = \hat{T}_i^0 e^{-b_u\left((m^*)^{a_U} - (M^*)^{a_U}\right)} \quad \text{for unloading, } \dot{m} < 0 \text{ from m=M.}$$

$$T_i = \hat{T}_i^0 e^{-b_R\left((m^*)^{a_R} - (M^*)^{a_R}\right)} \quad \text{for reloading, } \dot{m} < 0 \text{ and m<M} \tag{5.5}$$

The recovery parameter, b_R, was assumed to be constant, while the unloading parameter, b_U, is determined as from the maximum alignment, max η_i, constant C_U, and exponent α_U.

$$b_U(\max \eta) = \left(\frac{1}{\max \eta} \right)^{\alpha_U} C_U \tag{5.6}$$

Letting b_U decrease with increasing alignment seems to produce more realistic results. If b_U is constant, the unloading curve for higher subsequent stretches becomes unrealistically steep while intuition suggests that the unloading will become more gradual for materials that are more compacted. Assuming that b_U has a dependency on alignment, as in the above expression, a steeper "knock-down" factor can be used in the initial unloading curve while preventing an unrealistic response for the unloading at higher stretches. The model was evaluated for the deformation described above and the constant values given in Table 5.1. The corresponding stress-displacement response is shown in Figure 5.1.4.

Table 5.1.1 Constant values for model evaluation in Figure 5.1.4.

Variable	A	a_U	a_R	b_R	C	C_U	N	α_1	α_2	α_U	β	γ
Value	1.4	1.3	1.0	3	0.2	8	1	1.55	1.25	1	5.0E09	3.0

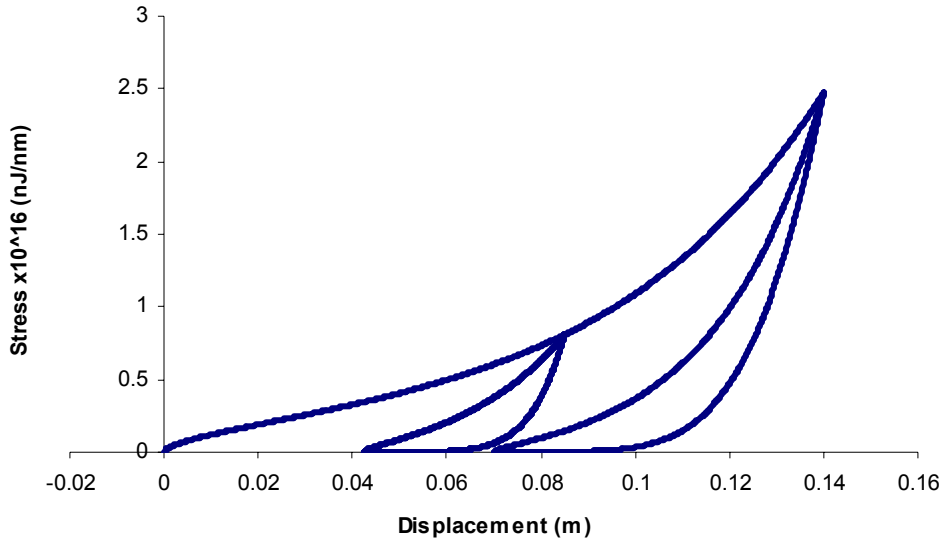

Figure 5.1.4 Stress-displacement results from the proposed model for multiple uniaxial compression cycles to different maximum stretches.

The predicted stress-displacement result in Figure 5.1.4 shows that the model successfully captures the irreversible deformation and hysteresis that are observed in the piston-cylinder tests for goose down (Figure 2.6.1). The forces were calculated at the end of each loading phase based on the cross-section of the spherical element and found to be 4.0 N and 12.0 N, respectively. These magnitudes are quite admissible based on the loads observed in the piston-cylinder test.

CHAPTER VI

CONCLUSIONS

6.1 Shortcomings of the Proposed Model

While orientation effects have been incorporated into the present model, treatment of slippage is indirectly accounted for by updating the reference configuration for the stretch free state. Perhaps, a more direct micromechanical means of incorporating slippage effects can be incorporated in future versions of the model.

The upturn at the end of the initial loading curve in the experimental result is not fully demonstrated in the present model. It is possible that additional configurations of constants will include this behavior; however, incorporation of more precise micromechanical relations into the strain-energy function would be more desirable. In particular, incorporating slippage effects that evolve with orientation will most likely help to capture this behavior.

6.2 Future Considerations

All of the relationships used in the proposed model presented here are based on assumptions regarding the microstructural dependency on deformation. Experiments should be sought to accurately quantify the relationships that describe the evolution of tertiary contacts and primary structure orientation with applied deformation. Developing such experiments is extremely difficult due to spatial variations within the material and the small scale of the tertiary structures. A more tractable way to study these features in

detail might be to develop a comprehensive finite element model for goose down analogous to the model that Beil and Roberts (2002A/B) formulated for wool.

Experiments also need to be done to better characterize the behavior of bulk goose down. The results of these experiments will help to better fit the proposed model and further identify any deficiencies. These experiments are also necessary to determine the behavior for subsequent loadings of increasing deformation, namely if the stress continues to increase along the original stress response or continues along the current response. These experiments will also better characterize the nature of the irreversible deformation observed which can then be used to better determine the shift in stress-free state.

The properties of the individual primary, secondary, and tertiary structures should also be explored. Some work has been done to study the tensile mechanical properties of the primary structures (Bonser 1999), but no work has been done to determine if the secondary properties are different as their behavior suggests. The small size of the secondary and tertiary structures makes them difficult to work with and test in conventional equipment designed for testing high-strength fibers or metals.

Several assumptions have been made in developing the model presented here that deserve further study. First, the material has been considered to be homogeneous. Due to the inherent heterogeneity of goose down, a purely micromechanical model should be implemented to incorporate effects of spatial distribution. One possible method for incorporating the spatial distribution would be to include a parameter analogous to the *floc* parameter used by Ostoja-Starzewski *et al.* (2000) in their model for paper. Spatial

distributions are likely to influence most of the mechanisms proposed in this model and are likely to be difficult to incorporate.

Viscoelastic rate dependencies have thus far been ignored and deserve considerations as the recovery phase is not necessarily immediate. The rate of deformation may also impact irreversibility and the evolution of the orientation distribution.

It is well known that moisture can inhibit the insulating abilities of goose down because it diminishes recovery (Bonser *et al.* 2001). An extremely comprehensive future model might include moisture effects. Capturing these effects would prove to be extremely challenging since the level of cleaning that the down undergoes impacts the susceptibility of goose down to moisture. Some untreated goose down samples are relatively unaffected by moisture because of the natural oils that are still present and rapidly repel moisture. Samples that have undergone repeated washings usually have smaller amounts of these natural oils and are affected by moisture. Therefore, incorporating moisture effects would necessitate further study into the treatments that goose down suppliers use and their effect on moisture absorption.

Goose down also exhibits a reaction to static charge. It was common to see primary structures become "attracted" to other down clusters as well as fingers and tweezers. Furthermore, the IDFL (2004) has reported detectable differences in fill power between samples that have been treated to minimize static change and those that have not. Even if the effect of static charge cannot be implemented into a computational model, studying its influence experimentally could provide valuable information on how

goose down should be "stuffed" into products or if certain casing materials would be more effective.

The data obtained by the IDFL (2004) (Figure 2.1.1) also suggests that there is a correlation between the fill power and the quality, or *content*, of a down sample. Incorporating some type of quality parameter into the model would be a nice feature. The *content* effect could be determined through further experiments on bulk goose down of different fill powers and their associated content. *Content* can probably be incorporated into the constant β, however, further study into any coupling between *content* and primary structure orientation and contact formation should be explored.

Lastly, the proposed model has assumed that all elastic strain-energy is stored in the secondary structures due to tertiary-to-tertiary contacts. The primary structures may contribute some elastic energy as well and might be included in future models. While tertiary-to-tertiary contacts were the most common interactions that resulted in appreciable secondary deformation, it is possible that there are some more complex interactions due to three or more secondaries coming into contact that also result in significant secondary deflections. Incorporating these other contact mechanisms into future revisions of this model might produce more accurate results.

6.3 Conclusions

The hierarchical structure of goose down contributes to its superior resilience. In particular, the tertiary structures provide stable points for contact to occur. This tertiary contact mechanism is significantly different from the contacts that occur with smooth fibers like wool. The tertiary structures provide a physical stop along the secondary

structure that allows tertiary-to-tertiary contacts to withstand a much greater load before slip occurs which is dramatically different from smooth fibers where only friction opposes slip. Due to this difference, goose down can probably store more elastic energy than smooth fiber systems like wool. These observations suggest that it might be beneficial to produce synthetic fibers that have a feature analogous to the tertiary structures.

The proposed model incorporates this tertiary contact mechanism and orientation effects into a unique strain-energy function. The orientation effects are included through the use of a fabric ellipsoid that greatly simplifies this model over the previous models that have incorporated orientation. This unique strain-energy function has been used to determine the principal stress during the initial loading of the material. This initial stress is used to determine the principal stress during unloading and reloading while including hysteresis and irreversible deformation. This model accomplishes reasonable results in a far more tractable manner than other models that have been proposed and is the first application to goose down specifically.

While the model developed here has been used explicitly to study goose down, the framework can be extended to many other materials that exhibit a similar behavior. In particular, the framework used to determine the stress in unloading and reloading can be extended to virtually any material for which the stress in the *virgin* material is known and might be used to capture the residual effects observed in cyclic loading of some rubbers.

REFERENCES

Beatty, M.F., Zúñiga, A.E., "A new phenomenological model for the stress-softening in elastomers.", *J. Appl. Math. Phys*. (*ZAMP*), 2002, v. 53, pp. 794-814

Beatty, M.F., Johnson, M.A., "The Mullins effect in uniaxial extension and its influence on transverse vibration of a rubber string", *Continuum Mech. Thermodyn.*,1993, v.5, pp 83-115

Beil, N.B. and Roberts, W.W., Jr., "Modeling and Computer Simulation of Compressional Behavior of Fiber Assemblies, Part I: Comparison to van Wyk's Theory", *Textile Res. J.*, 2002A, v. 72(4), pp. 341-351

Beil, N.B. and Roberts, W.W., Jr., "Modeling and Computer Simulation of Compressional Behavior of Fiber Assemblies, Part II: Hysteresis, Crimp, and Orientation Effects", *Textile Res. J.*, 2002B, v. 72(5), pp. 375-382

Bonser, R.H.C. and Dawson, C., "The Structural Mechanical Properties of Down Feathers and Biomimicking Natural Insulation Materials", *Journal of Materials Science Letters*, 1999, v. 18, pp1769-1770

Bonser, R.H.C., Farrent, J.W., "Influence Of Hydration On The Mechanical Performance Of Duck Down Feathers", *British Poultry Science*, 2001, v. 42, pp271-273

Carnaby, G.A. and Pan, N., "Theory of Compression Hysteresis of Fibrous Assemblies", *Textile Res. Inst.*, 1989, 59, pp275-284

Carrington, R., "Down and Out; A Buyer's Guide to Down Jackets and Sleeping Bags", The British Mountaineering Council, **Summit Issue 18**, pp31-33
http://www.thebmc.co.uk

Cowin, S.C., Turner, C.H., "Dependence of Elastic Constants of an Anisotropic Porous Material Upon Porosity and Fabric", *J. of Materials Sci.*, 1987, v. 22, n. 9, pp3178-3184

Cowin, S.C., "The Relationship Between the Elasticity Tensor and the Fabric Tensor", *Mech. of Materials*, 1985, v. 4(2) , pp137-147

Cox, H.L., "The Elasticity and Strength of Paper and other Fibrous Materials", *British Journal of Applied Physics*, 1952, v. 3, pp72-79

De Souza Neto, E.A., Perić, D., Owen, D.R.J., "A phenomenological three-dimensional rate-independent continuum model for highly filled polymers: formulations and computational aspects.", *J. Mech. Phys.* Solids, 1994, v42(10), pp1533-1550.

Dunlop, J.I., "Characterizing the Compression Properties of Fibre Masses", *Journal of Textile Institute*, 1974, v.65, pp532-536

Dunlop, J.I., "Acoustic Emission from Wool during Compression", *Journal of Textile Institute*, 1981, v.70, pp364-366

Dunlop, J.I., "The Dynamic Bulk Modulus of Fibre Masses", *Journal of Textile Institute*, 1981, v.72, pp154-161

Dunlop, J.I., "On the Compression Characteristics of Fibre Masses", *Journal of Textile Institute*, 1983, v.74, pp92-97

Flory, P.J. and Rehner, J., "Statistical Mechanics of Cross-Linked Polymer Networks", *The Journal of Chemical Physics*, 1943, v. 11, n. 11, pp512-520

Frisch-Fay, R., *Flexible Bars*, Butterworths, Washington, 1962

Gurtin, M.E., Francis, E.C., "Simple rate-independent model for damage", *J. Spacecraft*, 1981, v. 18(3), pp. 285-286

Hayter, A.J., *Probability and Statistics for Engineers and Scientists*, Wadsworth Group (Duxbury), Pacific Grove, CA, 2002

Holzapfel, G.A., "Nonlinear Solid Mechanics; A Continuum Approach for Engineering", John Wiley and Sons, West Sussex, 2000

International Down and Feather Laboratory (IDFL), www.idfl.com/articles, 2004

James, H.M. and Guth, E., "Theory of the Elastic Properties of Rubber", *The Journal of Chemical Physics*, 1943, v. 11(10), pp455-481

Komori, T., and Makishima, K., "Numbers of Fiber-to-Fiber Contacts in General Fiber Assemblies", *Textile Res. J.* , 1977, v. 47, pp13-17

Komori, T, and Itoh, M., "Estimation of Fiber Orientation and Length in Fiber Assemblies", *Textile Res. J.* , 1978, v. 48, pp309-314

Komori, T. and Itoh, M., "A New Approach to the Theory of the Compression of Fiber Assemblies", *Textiles Research Journal,* 1991, v. 61(7), pp420-428

Komori, T, and Itoh, M., "Theory of General Deformation of Fiber Assemblies", *Textile Research Journal*, 1991B, v.61(10), pp588-594

Lee, D.H. and Carnaby, G.A., "Compressional Energy of the Random Fiber Assembly; Part I: Theory", *Textiles Research Journal*, 1992, v. 62(4), pp185-191

Lee, D.H. and Carnaby, G.A., "Compressional Energy of the Random Fiber Assembly; Part II: Evaluation", *Textiles Research Journal*, 1992, v. 62(5), pp258-265

Malvern, L.E., "Introduction to the Mechanics of a Continuous Medium", Prentice-Hall Inc., Upper Saddle River, NJ, 1969

Marckmann, G., Verron, E., Gornet, L., Chagnon, G., Charrier, P., Fort, P., "A Theory of Network Alteration for the Mullins Effect", *Journal of Mech. and Phy. of Solids,* 2002, v. 50, pp 2011-2028

Mooney, M., "A Theory of Large Elastic Deformation", *Journal of Applied Physics*, 1940, v. 11, pp582-592

Mullins, L., and Tobin, N.R., "Theoretical model for the elastic behavior of filled-reinforced vulcanized rubbers", *J. Rubber Chem. Tech.*, 1957, v. 30, pp 555-571

Oda, M., Konishi, J., Nemat-Nasser, S., "Some Experimentally Based Fundamental Results on the Mechanical Behavior of Granular Materials", *Geotechnique*, 1980, v.30, pp479-495

Ogden, R.W., "Large Deformation Isotropic Elasticity - On the Correlation of Theory and Experiment for Incompressible Rubberlike Solids", *Proc. of the Royal Society of London. Series A, Mathematical and Physical Sciences*, 1972, v. 326, pp565-584

Ogden, R.W., and Roxburgh, D.G., "A Pseudo-Elastic model for the Mullins effect in filled rubber", *Proc. R. Soc. London. A*, 1999, vol 455, pp 2861-2877

Ostoja-Starzewski, M. and Stahl, D.C, "Random Fiber Networks and Special Elastic Orthotropy of Paper", *Journal of Elasticity*, 2000, v.60, pp131-149

Rivlin, R.S., "Large Elastic Deformations of Isotropic Materials IV. Further Developments of the General Theory", *Philosophical Transactions of the Royal Society of London. Series A, Mathematical and Physical Sciences*, 1948, v. 241, pp379-397

Shepherd, J.E., "An Internal State Variable Based Constitutive Model For Semi-Crystalline Polymers", Master's Thesis, Georgia Institute of Technology, 2002

Treloar, L.R.G., "The Physics of Rubber Elasticity", Oxford University Press, Oxford, 1975

Van Wyk, C.M., "Note on the Compressibility of Wool", *Journal of Textile Institute*, 1946, v. 37, ppT285-T292

UTHSCSA Image Tool, Freeware computer software, The University of Texas Health Science Center in San Antonio, 2002, downloadable via anonymous FTP from: ftp://maxrad6.uthscsa.edu